Title
Modeling Coupled THM Processes and Brine Migration in Salt at High Temperatures:

Authors
Rutqvist, Jonny
Blanco-Martin, Laura
Molins, Sergi
et al.

Publication Date
2015-09-18

Modeling Coupled THM Processes and Brine Migration in Salt at High Temperatures

Fuel Cycle Research & Development

Prepared for

U.S. Department of Energy
Used Fuel Disposition Campaign

Jonny Rutqvist
Laura Blanco-Martín
Sergi Molins
David Trebotich
Jens Birkholzer
Lawrence Berkeley National Laboratory

September 2015

FCRD-UFD-2015-000366
LBNL-191216

Revision 2
12/20/2012

APPENDIX E

FCT DOCUMENT COVER SHEET [1]

Name/Title of Deliverable/Milestone/Revision No.	Modeling Coupled THM Processes and Brine Migration in Salt at High Temperatures
Work Package Title and Number	DR Salt R&D - LBNL FT-15LB081801
Work Package WBS Number	1.02.08.18
Responsible Work Package Manager	Jens Birkholzer (signature on file) (Name/Signature)

Date Submitted 9/18/2015

Quality Rigor Level for Deliverable/Milestone[2]	☐ QRL-3	☐ QRL-2	☐ QRL-1 ☐ Nuclear Data	☒ Lab/Participant QA Program (no additional FCT QA requirements)

This deliverable was prepared in accordance with Lawrence Berkeley National Laboratory
(Participant/National Laboratory Name)

QA program which meets the requirements of
☒ DOE Order 414.1 ☐ NQA-1-2000 ☐ Other

This Deliverable was subjected to:

☐ Technical Review ☐ Peer Review

Technical Review (TR)

Review Documentation Provided
☐ Signed TR Report or,
☐ Signed TR Concurrence Sheet or,
☐ Signature of TR Reviewer(s) below

Peer Review (PR)

Review Documentation Provided
☐ Signed PR Report or,
☐ Signed PR Concurrence Sheet or,
☐ Signature of PR Reviewer(s) below

Name and Signature of Reviewers

_____ _____

_____ _____

_____ _____

NOTE 1: *Appendix E should be filled out and submitted with the deliverable. Or, if the PICS:NE system permits, completely enter all applicable information in the PICS:NE Deliverable Form. The requirement is to ensure that all applicable information is entered either in the PICS:NE system or by using the FCT Document Cover Sheet.*

NOTE 2: *In some cases there may be a milestone where an item is being fabricated, maintenance is being performed on a facility, or a document is being issued through a formal document control process where it specifically calls out a formal review of the document. In these cases, documentation (e.g., inspection report, maintenance request, work planning package documentation or the documented review of the issued document through the document control process) of the completion of the activity along with the Document Cover Sheet is sufficient to demonstrate achieving the milestone. If QRL 1, 2, or 3 is not assigned, then the Lab/Participant QA Program (no additional FCT QA requirements) box must be checked, and the work is understood to be performed, and any deliverable developed, in conformance with the respective National Laboratory/Participant, DOE- or NNSA-approved QA Program.*

Intentionally Left Blank

CONTENTS

FIGURES

TABLES

ACRONYMS

DOE	Department of Energy
DRZ	Disturbed Rock Zone
EBS	Engineered Barrier System
EDZ	Excavation Damaged Zone
EOS	Equation-Of-State
FEPs	Features, Events and Processes
GSR	Generic Salt Repository
LANL	Los Alamos National Laboratory
LBNL	Lawrence Berkeley National Laboratory
NBS	Natural Barrier System
NCG	Non-condensable Gas
PWR	Pressurized Water Reactor
R&D	Research & Development
REV	Representative Elemental Volume
THM	Thermal-Hydrological-Mechanical
THMC	Thermal-Hydrological-Mechanical-Chemical
TM	Thermal-Mechanical
TSDE	Thermal Simulation for Drift Emplacement
TUC	Clausthal University of Technology, Germany
UFD	Used Fuel Disposition
UFDC	Used Fuel Disposition Campaign
WIPP	Waste Isolation Pilot Plant

1. INTRODUCTION

In this report, we present FY2015 progress by Lawrence Berkeley National Laboratory (LBNL) related to modeling of coupled thermal-hydrological-mechanical-chemical (THMC) processes in salt and their effect on brine migration at high temperatures. This is a combined milestone report related to milestone Salt R&D Milestone "Modeling Coupled THM Processes and Brine Migration in Salt at High Temperatures" (M3FT-15LB0818012) and the Salt Field Testing Milestone (M3FT-15LB0819022) to support the overall objectives of the salt field test planning.

LBNL's work on the modeling of coupled THMC processes in salt was initiated in FY2012, focusing on exploring and demonstrating the capabilities of an existing LBNL modeling tool (TOUGH-FLAC) for simulating temperature-driven coupled flow and geomechanical processes in salt. This work includes development related to, and implementation of, essential capabilities, as well as testing the model against relevant information and published experimental data related to the fate and transport of water. An important component in this work is LBNL's collaboration with a research group led by Professor Lux at Clausthal University of Technology (TUC) in Germany, a world-leading research institution in salt geomechanics. The DOE UFD campaign and LBNL greatly benefit from TUC's experience in salt geomechanics and modeling of salt thermal-mechanical (TM) processes using FLAC3D. Conversely, TUC benefits from LBNL's expertise in modeling multiphase and heat transport processes at high temperature with TOUGH2 as well as LBNL's experience with the TOUGH-FLAC simulator for the modeling coupled THM processes in nuclear waste isolation. By leveraging on existing complementary capabilities of the LBNL and TUC, we have within a few years been able to develop and validate an advanced numerical simulation tool for modeling of coupled THM processes in salt and have demonstrated its applicability to nuclear waste isolation.

In FY2013 the work was focused on implementation and testing of constitutive models for salt host rocks and crushed salt. In particular, we implemented the Lux/Wolters model for modeling of creep, damage, sealing, and healing of the salt as a function of stress, temperature, and pore pressure. Moreover, we used the TOUGH-FLAC code with this newly implemented model together with other constitutive models for crushed salt backfill, and successfully completed model simulations of a generic salt-based repository over 100,000 years of simulation time. We developed and tested alternative ways for modeling hydraulic and mechanical coupling under large strain, including compaction of crushed salt from 30% porosity to a state equivalent to the solid host rock.

In FY2014 LBNL's work was focused on continued testing, application, and improvement of the computational models and tools to simulate high temperature coupled processes and their effect on brine accessibility and migration. This included improvements to the TOUGH-FLAC simulator related to implemented constitutive models for both solid rock salt and crushed salt, as well as related to the use of a Voronoi discretization for improved accuracy in the flow sub-problem. The Voronoi discretization is implemented to handle mesh deformation over time due to creep and the large strains associated with the mechanical behavior of the system. Based on these model improvements, updated simulations of long-term THM behavior of a generic repository was performed and we conducted code benchmarking in collaboration with the TUC research team. Work was also initiated for development of a dual-continuum approach for brine migration (involving both intercrystalline flow and intracrystalline brine inclusions).

The FY2015 we have conducted further verification, validation, application, of the TOUGH-FLAC model, initiated pore-scale (or micro-) modeling of salt inclusion migration, as well as several publications of our work in international peer-reviewed journals. The model development of TOUGH-FLAC for salt has reached sufficient maturity for state-of-the-art applications on coupled THM processes in salt, and therefore we are able to showcase the work and contribute to the state-of-the-sciences in the international salt research community in peer-reviewed publications. Along with improvement of the models and availability of new salt THM experimental data, we have been updating our generic repository THM model and conducted updated simulations of the long-term THM behavior. This includes updated two phase flow properties, capillary pressure curves, which are generally not available for natural salt, and improved modeling of water filtration induced at high pore-pressure. Two journal papers published in FY2015 are:

- Blanco-Martín et al. (2015) "Long-term modelling of the thermal-hydraulic-mechanical response of a generic salt repository for heat-generating nuclear waste" in Engineering Geology.
- Blanco-Martín et al. (2015) "Comparison of two simulators to investigate thermal-hydraulic-mechanical processes related to nuclear waste isolation in saliniferous formations" in Computers and Geotechnics.

Another major accomplishment in FY2015 is the first full 3D (86,000 elements) TOUGH-FLAC modeling of a salt repository (heater experiment); it is the modeling of the Thermal Simulation for Drift Emplacement (TSDE) test that was a major multi-year heater experiment conducted at Asse Mine in Germany in the 1990s. This is the first time this experiment has been modeled in a complete THM analysis (previous analyses of TSDE have been limited thermal-mechanical processes, ignoring multiphase flow hydraulic processes. The modeling of the TSDE also provides the opportunity to calibrate of stationary creep parameters at very low deviatoric stress and extremely slow loading that are not available from current laboratory tests. Good agreement was achieved between modeled and experimental data, involving drift closure and compaction of the EBS (crushed salt), thus providing validation of both host rock and crushed salt constitutive models and their implementation into the TOUGH-FLAC simulator.

In FY2015 we have also extended TOUGH-FLAC for considering salt precipitation and dissolution, including an improved TOUGH2 equation-of-state module. This model capability was demonstrated for the generic repository model, showing the evolution of porosity in the EBS as a function of both salt precipitation and mechanical compaction, affected by the thermal gradient and two-phase flow heat pipe effects. This model capability is currently being validated against laboratory data involving experiments with thermal gradient and monitoring of moisture content and porosity evolution.

Finally, in FY2015, LBNL has continued the work on the development of a constitutive model for migration of brine inclusions considering both pressure and thermal gradients. As part of this development LBNL has in FY2015 initiated pore-scale modeling of brine inclusion migration in salt crystals under thermal gradients. In this approach, the brine inclusions are modeled explicitly, including reactive mass transport under thermal gradient with dissolution and precipitation at hot and cold faces of the inclusions. The governing equations were implemented in the Chombo-Crunch code, which uses an embedded boundary-algebraic multigrid formulation

based on a finite volume discretization. The experiments reported by Caporuscio et al. (2013) have served as conceptual basis for the development of our pore scale model. Ongoing work is focusing on calibration of reactive parameters to match observed migration rates in these experiments.

Within the Natural Barrier System (NBS) group of the Used Fuel Disposition (UFD) Campaign at DOE's Office of Nuclear Energy, LBNL's research activities have focused on understanding and modeling coupled processes and impacts of the EDZ and high-temperature on parameters and processes relevant to performance of a salt repository. This report documents results from some of these activities. These activities address key Features, Events and Processes (FEPs), which have been ranked in importance from medium to high, as listed in Table 7 of the *Used Fuel Disposition Campaign Disposal Research and Development Roadmap* (FCR&D-USED-2011-000065 REV0) (Nutt, 2011). Specifically, they address FEP 2.2.01, Excavation Disturbed Zone, for salt, by investigating how coupled processes affect EDZ evolution; FEP 2.2.05, Flow and Transport Pathways; FEP 2.2.08, Hydrologic Processes; and FEP 2.2.07, Mechanical Processes by studying near-field coupled THM processes in salt repositories. The activities documented in this report also address a number of research topics identified in *Research & Development (R&D) Plan for Used Fuel Disposition Campaign (UFDC) Natural System Evaluation and Tool Development* (Wang, 2011), including Topics S3, Disposal system modeling – Natural system; P14, Technical basis for thermal loading limits; and P15 Modeling of disturbed rock zone (DRZ) evolution (salt repository).

In the following Section 2 of this report, we provide more details on the FY2015 work related to brine migration modeling in support of thermal field testing, work that has been focused on the modeling of the TSDE experiment. This is followed in Section 3 with details on work related to R&D on salt migration modeling, including improved generic repository modeling, extension to consider halite dissolution and precipitation, and validation against laboratory experiments such as LANL's heating in a pile of crushed salt. The work initiated on pore-scale modeling is presented in a separate Section 4, as this was conducted in support of both the salt field testing and R&D work. We conclude with an outlook for FY2016 proposing a work scope to continue to test and apply computational models and tools to simulate coupled THM processes and brine migration in salt.

2. BRINE MIGRATION MODELING IN SUPPORT OF A THERMAL FIELD TEST

2.1 Introduction

In FY2014 (Rutqvist et al., 2014), we presented preliminary THM modeling results of the TSDE (*Thermal Simulation for Drift Emplacement*) test. During FY2015, we have extensively modeled this test, including inverse modeling and parameter estimation as will be shown. The main results are presented in this section, after a short description of the test and its main features. Most of the modeling activities related to the TSDE test have been performed in collaboration with Clausthal University of Technology, Germany. In addition to beneficial scientific exchanges, this fruitful collaboration has allowed us to benchmark two simulators for coupled flow and geomechanics processes, TOUGH-FLAC and FLAC-TOUGH, suitable to investigate the underground disposal of heat-generating nuclear waste. At LBNL, the updated TOUGH-FLAC simulator for large strains and creep processes is used. We recall that the TSDE simulations are three-dimensional because previous thermal and thermo-mechanical modeling of the TSDE experiment confirmed

the need for a 3D model, at least for the determination of the temperature field (Bechthold et al., 1999).

2.2 Short description of the TSDE experiment

The *Thermal Simulation for Drift Emplacement* (TSDE) experiment was conducted in the Asse salt mine in Germany in the 1990s to support the development of the in-drift emplacement concept with multiple barriers (Bechthold et al., 1999; 2004). One significant aspect of the TSDE experiment is that it was extensively monitored, using several observation and access drifts, as well as more than 200 boreholes for instrumentation, with sensors scanned every 12 hours. The extensive measurement program included temperature, drift closure, rock deformation, stress evolution, and gas generation and transport, among others. Some measuring devices were specially designed for this experiment. Therefore, in addition to evaluating the feasibility of the in-drift emplacement concept, the TSDE experiment provided a vast database on relevant phenomena and processes regarding the host rock, the backfill, and also the waste packages. Subsequent analysis of the observations led to an improved understanding of the behavior of the host rock and the backfill under reference repository conditions for heat-generating nuclear waste, as well as to the development and improvement of constitutive models and computer codes required to predict the aforementioned relevant phenomena and processes (Bechthold et al., 1999).

In the TSDE experiment, six electrical heaters were placed in two parallel drifts excavated for the purposes of the experiment in the 800 m level of the Asse mine, in the North-Eastern part of the salt dome. The drifts were excavated in a relatively undisturbed area (Staβfurt Halite of the Zechstein series), and three heaters were emplaced in the central part of each drift. The left-hand side image in Figure 2-1 shows the Asse salt dome and the location of the TSDE experiment, and the right-hand side image shows a view of the two test drifts. Some observation drifts (750 m level) and boreholes can also be seen in the image.

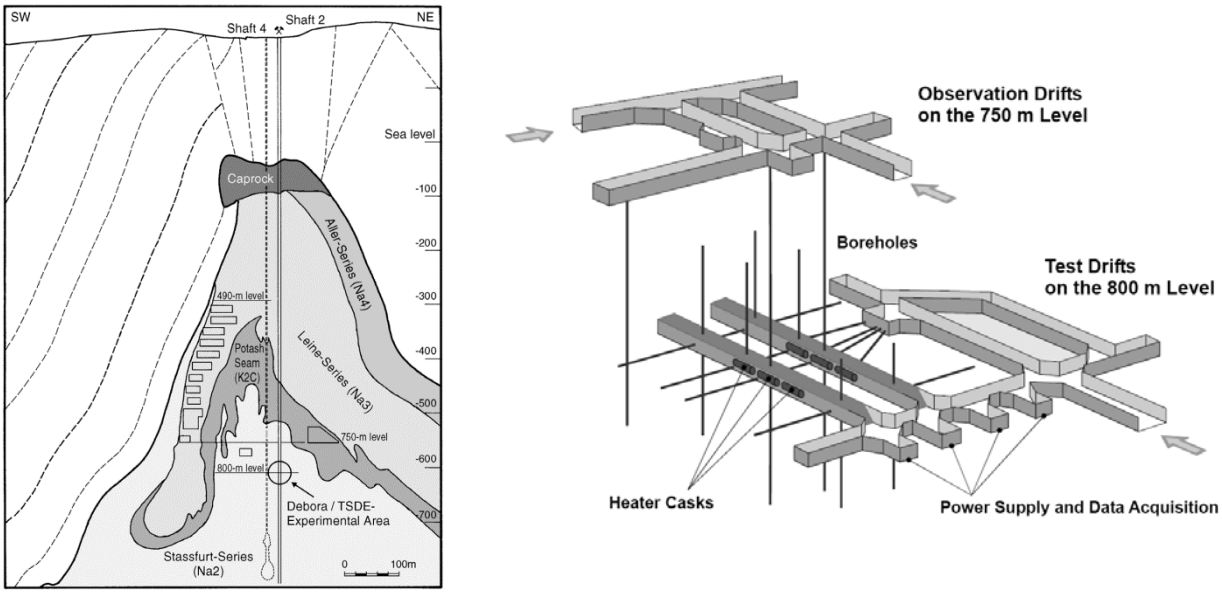

Figure 2-1. TSDE test: (a): cross-section of the Asse salt mine, indicating the location of the TSDE experiment; (b): schematic representation of the test area.

The dimensions of the drifts, as well as the heat capacity of the electrical heaters, were selected to match the preliminary layout of the in-drift emplacement concept; therefore, the test represented a portion of a typical repository emplacement panel. The heaters were 5.5 m long, had a diameter of 1.6 m and were separated by 3 m along the drift axis. They weighted about 65 t, and their design was based on POLLUX casks for 8 pressurized water reactor (PWR) assemblies. The drifts were about 4.5 m wide and 3.5 m high, and had a length of 77 m. A 10 m wide pillar lay between them. The heaters were emplaced 1.4 years after excavation. Immediately after the emplacement of the heaters, the drifts were backfilled using crushed salt, sieved to exclude grain sizes larger than 45 mm. The heaters were switched on in September 1990 and a constant heat load of 6.4 kW was applied to each heater until February 1999. At that date, the heaters were switched off. The measuring instruments were installed in twenty monitoring cross-sections, not only in the heated area, but also in the non-heated area of the two drifts. Figure 2-2 displays a plan view of the two drifts, including instrumented cross-sections.

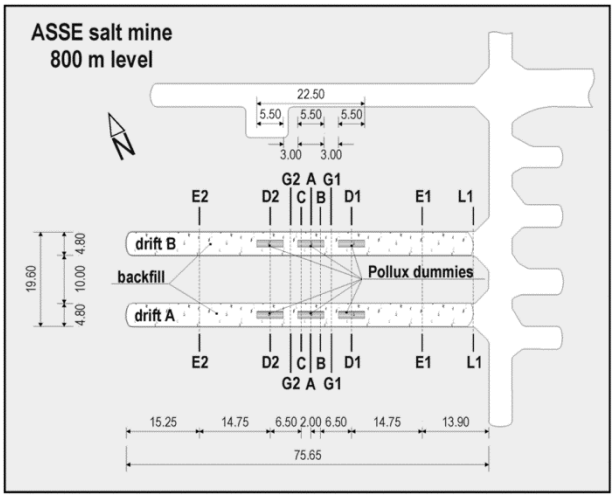

Figure 2-2. TSDE test: plan view of the test drifts and of the monitoring cross-sections.

As compared to previous numerical exercises of the TSDE test (Bechthold et al., 1999, Pudewills and Droste, 2003), in our simulations we include transient, damage and healing processes within the natural salt, and we also account for hydraulic processes. Indeed, most of the previous numerical studies concentrated on thermo-mechanical analyses due to the dominant influence of heating, and its effect on the mechanical response of the host rock and the backfill. Those studies were one-way coupled (from heat flow to mechanics) or two-way coupled, depending on the computational resources available. The THM simulations presented in this paper are two-way coupled, and account for material-specific characteristics of salt rock mass and crushed salt (Blanco-Martín et al 2015a; b).

2.3 Model description, initial and boundary conditions

According to the geometry of the TSDE experiment (see Figure 2-1 and Figure 2-2), we have prepared a three-dimensional model of half of one drift, with two symmetry planes: one at X=0 (across the pillar between the two test drifts) and one at Y=0 (across the central cross-section of the drifts). Our model is 100 m wide, 200 m high and 38.5 m deep. Figure 2-3 shows some views of the initial discretization used in geomechanics, including important dimensions. In Figure 2-4, some views of the corresponding Voronoi partition are displayed. We recall that we use the software library Voro++ (Rycroft, 2009) to compute the Voronoi tessellation corresponding to the centroids of a FLAC^{3D} mesh. All external planes are no-flow boundaries. Additionally, the displacement is blocked in the normal direction to those planes. The mesh has 85,870 elements.

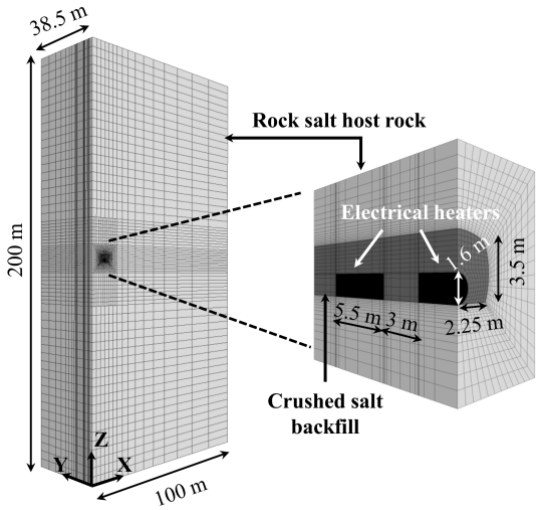

Figure 2-3. TSDE test: views of the initial mesh used in the geomechanics sub-problem. The main dimensions of the model are also shown.

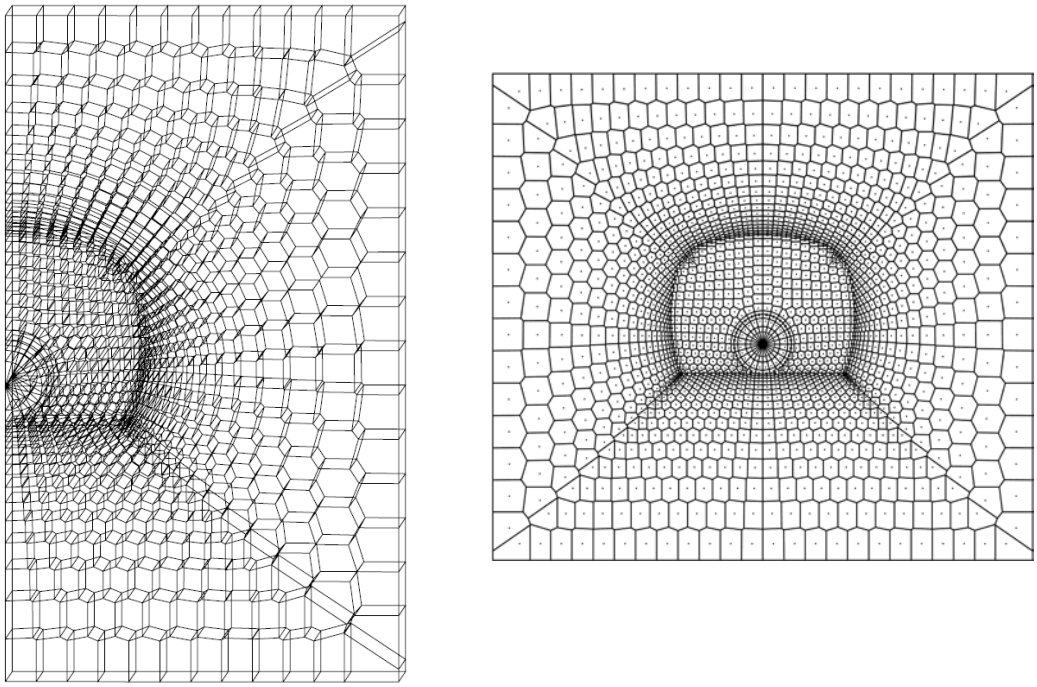

Figure 2-4. TSDE test: views of the initial mesh used in the flow sub-problem. To make the visualization easier, only the drift area is displayed. In the left-hand side figure, only one column of elements along the *Y* axis is shown.

Based on available information, we assign an initial stress field of 12 MPa to the host rock (isotropic). The initial pore pressure within the natural salt is lithostatic, and the initial temperature is 36.4 °C. Table 2-1 lists relevant flow and mechanical parameters of the host rock

and the crushed salt. We highlight that, apart from the grain density, the linear thermal expansion coefficient, and the relative permeability parameters, these properties evolve during the simulation as detailed in (Blanco-Martín et al., 2015a; b). For code-to-code verification and benchmark purposes, the evolution of the properties is the same in TOUGH-FLAC and FLAC-TOUGH, i.e., only the numerical scheme is different. As compared to Blanco-Martín et al. (2015a), here the only difference is the model used for the evolution of thermal conductivity. Based on information from the BAMBUS project (Bechthold et al., 1999; 2004), for the natural salt we use

$$\lambda_{\text{salt}} = 6.138 - 2.248 \cdot 10^{-2} T + 3.627 \cdot 10^{-5} T^2 + 1.0 \cdot 10^{-9} T^3 \qquad (2.1)$$

where λ is thermal conductivity [W/m·K] and T is temperature [°C].

For the crushed salt, we use

$$\lambda_{\text{crushed salt}} = \max\left(\frac{\phi}{\phi_0}\lambda_{\text{crushed salt},0} + \left(1 - \frac{\phi}{\phi_0}\right)^m \lambda_{\text{salt}}, 0.8\right) \qquad (2.2)$$

where ϕ [-] is the current crushed salt porosity, ϕ_0 [-] is the initial crushed salt porosity, and m=1.1. Moreover,

$$\lambda_{\text{crushed salt},0} = 4.758 \cdot 10^{-1} + 8.532 \cdot 10^{-4} T + 1.048 \cdot 10^{-6} T^2 - 2.222 \cdot 10^{-9} T^3 \qquad (2.3)$$

Table 2-1. Mechanical and flow properties of the crushed salt and the natural salt.

Property [unit]	Crushed salt	Rock salt
Bulk modulus, K [MPa]	150[a]	17,390[b]
Shear modulus, G [MPa]	70[a]	9450[b]
Initial Biot coefficient, α [-]	1[a]	0.003[b]
Porosity ϕ [-]	0.35[a]	0.002[b]
Permeability, k [m^2]	$5.8 \cdot 10^{-13}$[a]	0[b]
Initial thermal conductivity (36.4 °C) [$W \cdot m^{-1} \cdot K^{-1}$]	0.8[a]	5.36[c]
Initial heat capacity (36.4 °C) [$J \cdot kg^{-1} \cdot K^{-1}$]	860[c]	860[c]
Initial liquid saturation, S_l [-]	0.02	0.5
Grain density, ρ [$kg \cdot m^{-3}$]	2154	2154
Linear thermal expansion coeff., α_T [K^{-1}]	$4.2 \cdot 10^{-5}$	$4.2 \cdot 10^{-5}$
Relative permeability functions	Corey	Corey
Residual liquid saturation, S_{lr} [-]	0.05	0.05
Residual gas saturation, S_{gr} [-]	0	0

[a] non-constant value (changes during reconsolidation);
[b] damage- and healing- dependent value;
[c] temperature-dependent property

As for the electrical heaters, we assume linear elasticity and standard properties of stainless steel. The flow and mechanical properties used for steel are kept constant during the simulation. The heat load of each heater (6.4 kW) is distributed proportionally to the volume of the grid-blocks used as heat sources.

From the flow point of view, we model two-phase flow of water and air, both by diffusion and advection. Heat flow occurs by conduction and convection. TOUGH2 Equation-Of-State (EOS) 3 has been used. Diffusive mass transport of vapor and air is modeled with coefficients that depend on pressure and temperature (Vargaftik, 1975), and tortuosity effects are accounted for using the Millington and Quirk model (1961).

From the mechanical point of view, the time-dependent response of the natural salt is described using the *Lux/Wolters* constitutive model, which allows modeling elastic, visco-plastic, damage and healing processes characteristic of rock salt (Hou, 2003; Wolters et al., 2012). This state-of-the-art constitutive model has been validated against field and experimental data and has been implemented in FLAC^{3D} as a user-defined model. The total strain rate tensor reads

$$\dot{\varepsilon}_{ij} = \dot{\varepsilon}_{ij}^{e} + \dot{\varepsilon}_{ij}^{vp} + \dot{\varepsilon}_{ij}^{d} + \dot{\varepsilon}_{ij}^{h} \qquad (2.4)$$

where superscripts *e*, *vp*, *d*, and *h* stand for elastic, viscoplastic, damage, and healing, respectively. All the components of the strain rate tensor defined in Eq. (2.4) take a damage-induced reduction of the load-bearing cross-sectional area into account, in accordance with a previous study (Kachanov, 1986). The parameters of the *Lux/Wolters* model used in this research have been determined from the interpretation of experimental results (Lerche, 2012). As will be explained in Section 2.5, three parameters that describe Maxwell viscosity (stationary creep) have been adjusted to the available experimental data of the TSDE test, because their correct determination at laboratory-scale requires very long test durations.

For the crushed salt, we use a modified version of the *cwipp* model (a crushed salt creep model originally developed for the waste isolation plant, New Mexico) implemented in FLAC^{3D} (Itasca, 2012; Sjaardema and Krieg, 1987). The main characteristic of the *cwipp* model is that it allows modeling time-dependent volumetric strain changes. While density is not allowed to decrease in the *cwipp* model during reconsolidation (i.e., density is a monotonically increasing function), it honors the volumetric strain evolution in our modified version. The total strain rate tensor reads

$$\dot{\varepsilon}_{ij} = \dot{\varepsilon}_{ij}^{e} + \dot{\varepsilon}_{ij}^{vc} + \dot{\varepsilon}_{ij}^{vs} \qquad (2.5)$$

where superscripts *e*, *vc*, and *vs* stand for elastic, viscous compaction and viscous shear, respectively. For our simulations, we initially used parameters available in the literature (DBE 2001; Itasca, 2012). Then, in order to achieve a better prediction, the parameters of the compaction part were recalibrated, as will be explained in Section 2.5.

2.4 Modeling sequence

First, the initial equilibrium and drift excavation are modeled. The excavation is assumed instantaneous, and flow during this stage is disregarded. The coupled THM simulations performed include two parts: (1) the open drift phase, before the emplacement of the electrical heaters and subsequent backfilling of the drifts (1.4 years), and (2) the experiment itself (heating), which lasted 8 years and 5 months.

During the open drift phase, the heaters and backfill are de-activated and the pore pressure is kept constant within the drift at 0.1 MPa. During this phase, the temperature remains about constant. The main purpose of modeling this phase is to investigate the mechanical response of the natural salt (transient, stationary and tertiary creep), including the excavation damage zone. After 1.4 years, the heaters and backfill are activated. The initial porosity of the backfill is 35%, and the initial pore pressure and temperature within the drift are 0.1 MPa and 36.4 °C, respectively (Bechthold et al., 1999). In accordance to the situation sketched in Figure 2-2, the extremity of the drift at Y=38.5 m is kept hydraulically open at the atmospheric pressure as a boundary condition during the heating phase. This leads to the effect that the pore pressure increase within the crushed salt induced by its compaction as well as by the heating of the included pore fluid is accompanied by a pore pressure decrease induced by an outflow of fluid at the open drift end. Therefore, pore pressure cannot increase very much within the drift.

Both during the open drift and excavation phases, the mesh is updated in the flow sub-problem progressively as the mesh used in the geomechanics sub-problem deforms. This operation is performed up to 50 times during the simulations.

Finally, we note that, in order to compute the effective stress tensor (geomechanics sub-problem), we use the saturation-averaged sum of the phase pressures computed in the flow sub-problem.

2.5 Results and discussion

In this section, we compare results obtained by TOUGH-FLAC (LBNL [Ruqvist et al., 2002]) and FLAC-TOUGH (TU Clausthal [Lux et al., 2014]). We also present the inverse modeling approach undertaken to determine a parameter set for the *cwipp* model (compaction part) that reproduced satisfactorily experimental backfill stress measurements. Additionally, the re-calibration of three parameters of the stationary creep of the natural salt is discussed.

2.5.1 Open Drift phase: general remarks

Due to a higher number of relevant processes occurring during the heating phase, most of the experimental data and analyses are concentrated on that period. However, a few aspects occurring during the open drift phase should be mentioned. Average vertical convergence rates were about 0.3%/year, and average horizontal convergence rates were about 0.25%/year. Our simulation results are in very good agreement with those rates (results are displayed in the next sub-section, Figure 2-10). In addition, our results suggest that the transient creep of the natural salt host rock finishes during this phase. Moreover, due to the stress redistribution induced by the excavation, the dilatancy boundary (Hou, 2003; Popp et al., 2001; Wolters et al., 2012) is exceeded and an excavation damaged zone (EDZ) develops around the drift. It extends about 1.5 m below the drift floor (flat floor), 0.8 m above the roof and 0.75 m beyond the sidewalls. Experimental evidence from the TSDE experiment (Bechthold et al., 2004) is in agreement with these EDZ characteristics. In the EDZ, permeability increases up to four orders of magnitude, and porosity reaches as high values as 0.7%. Secondary permeability within rock salt is calculated using a non-linear expression that accounts for dilatancy, effective stresses and their orientation (Blanco-Martín et al., 2015a).

2.5.2 Heating phase: temperature

Figure 2-5 displays the evolution of temperature at several locations within the backfill, in a cross-section containing a heater cask (section B in Figure 2-2). The temperature at the heater cask surface is included in the plot; it reached 210 °C five months after the beginning of heating, and it decreased thereafter as the thermal conductivity of the backfill increased (due to compaction), which facilitated the heat flow. The temperature increase was more gradual within the backfill, and significant temperature gradients were measured due to non-uniform compaction (which yields non-uniform thermal conductivity according to Eqs. (2.2-2.3)). After about 5 years, temperatures in the heater cask area reached a steady state (160-180 °C at the heater surface), while they continued to increase within the backfill at farther distances from the heater.

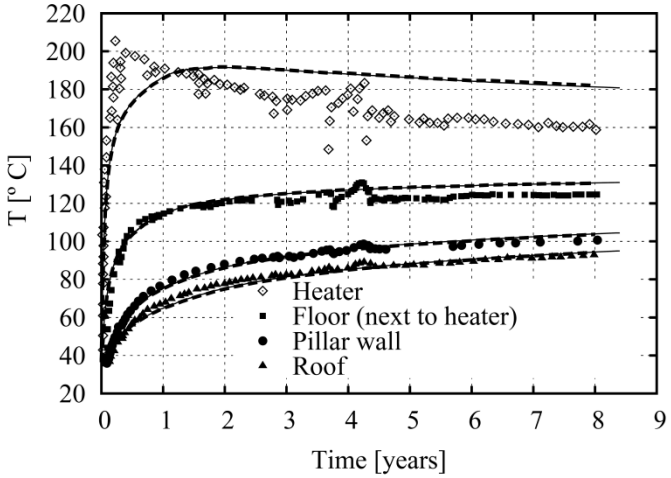

Figure 2-5. TSDE test: temperature evolution within the backfill (section B), and at the heater surface. Points represent measurements, solid lines correspond to TOUGH-FLAC and dashed lines correspond to FLAC-TOUGH.

In Figure 2-5, numerical predictions from TOUGH-FLAC and FLAC-TOUGH are also displayed. As the figure shows, results from the two simulators are in very good agreement between them. The predictions reproduce the measurements closely, with highest error at the heater surface. We note that we have performed THM simulations using two different forms for the evolution of thermal conductivity within the crushed salt; indeed, because most of the heater surface is in contact with crushed salt, the thermal conductivity of the backfill affects temperature at the heater surface. The two forms used have been derived from experimental data (Bechthold et al., 2004). One form is given by Eq. (2.3), and the other one is given by

$$\lambda_{\text{crushed salt}} = -270\phi^4 + 370\phi^3 - 136\phi^2 + 1.5\phi + 5 \qquad (2.6)$$

As opposed to Eq. (2.3), in Eq. (2.6), λ is only a function of porosity. Both functional forms are displayed in Figure 2-6, for porosity and temperature ranges relevant to the TSDE experiment. The simulation results issued from the use of Eq. (2.3) or Eq. (2.6) are very similar, showing only some small differences in the temperature evolution of the heater casks during the last years, due to the differences in thermal conductivity of the backfill at small porosities and high temperatures (see Figure 2-6).

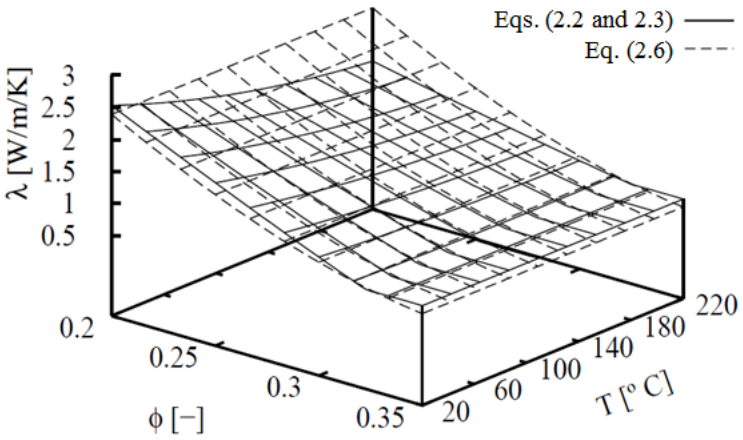

Figure 2-6. TSDE test: comparison of two empirical expressions to determine the thermal conductivity of compacting crushed salt. Both expressions have been proposed previously (Bechthold et al., 2004).

Figure 2-7 shows temperature evolution in additional monitored positions within the backfill: some of them in the heated area (1 m west of sections G2 and B in Figure 2-2) and some in the cold area (section E2 in Figure 2-2). Again, the results issued from the two simulators are in very good agreement, and they match the measurements quite well. The discrepancies observed, in particular for the curve labelled "2.2 m from floor," are likely due to local effects: local porosity variations can lead to changes in the thermal conductivity computed, and therefore to different temperatures. But overall, the predictions reproduce the temperatures measured quite well.

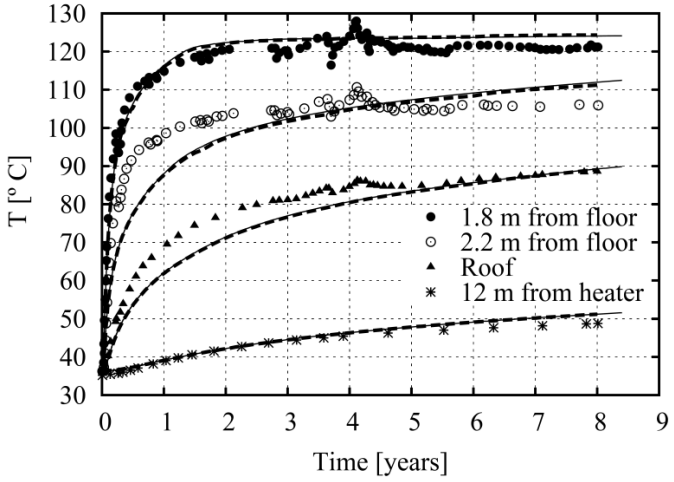

Figure 2-7. TSDE test: temperature evolution within the backfill (filled symbols refer to a section located 1 m west of section G2 and non-filled symbols refer to a section located 1 m west of section B. The curve labelled "12 m from heater" corresponds to the floor in section E2). Points represent measurements, solid lines correspond to TOUGH-FLAC and dashed lines correspond to FLAC-TOUGH.

Figure 2-8 (a) displays the temperatures within the rock, in the heated area (section A in Figure 2-2), and Figure 2-8 (b) displays rock temperatures in the non-heated area (section E1). Heat transfer towards the salt rock mass occurs both by direct contact between the heater cask and the drift floor (heated area only), and also through the backfill and the natural salt. As expected, temperature decreases with the increase in depth. While in the heated area temperatures reach a steady state after about 5 years (equilibrium between heat generation and propagation), temperature continues to increase in the cold area (progressive heat propagation). As both figures show, results from TOUGH-FLAC and FLAC-TOUGH are in very good agreement between them, and also with experimental data.

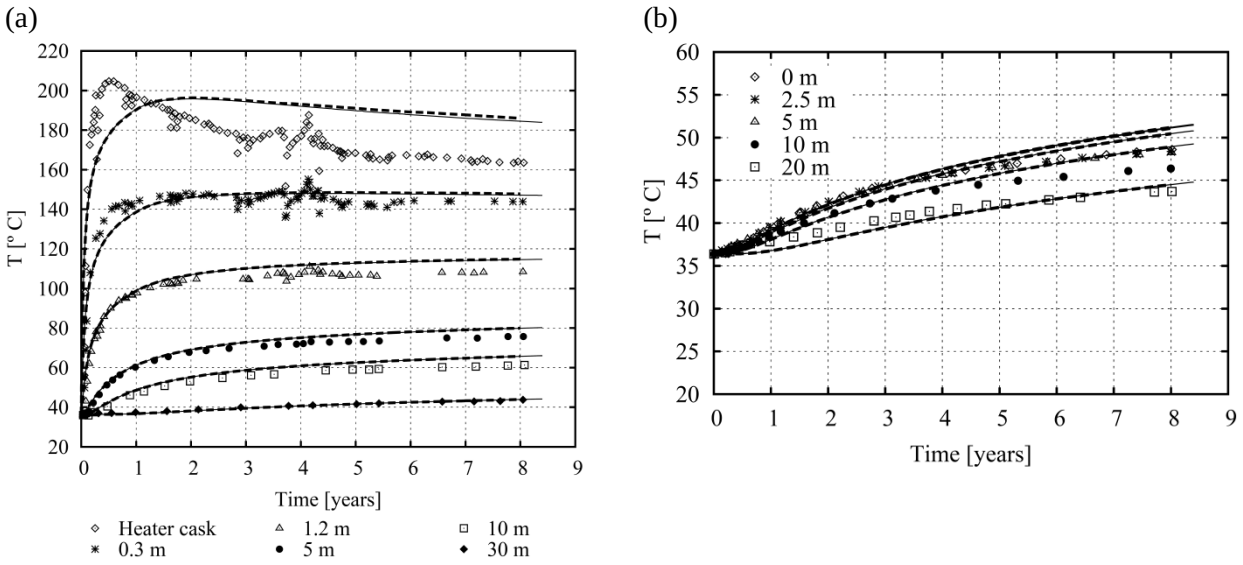

Figure 2-8. TSDE test: temperature evolution within the host rock, beneath the floor in (a) section A, and, (b) section E1. Points represent measurements, solid lines correspond to TOUGH-FLAC and dashed lines correspond to FLAC-TOUGH.

Finally, the rock temperatures between the two drifts, in the heated area (section A) are displayed in Figure 2-9. In this case, heat flow to the salt rock mass occurs mainly through the backfill. Again, we obtain a very good prediction of the measurements.

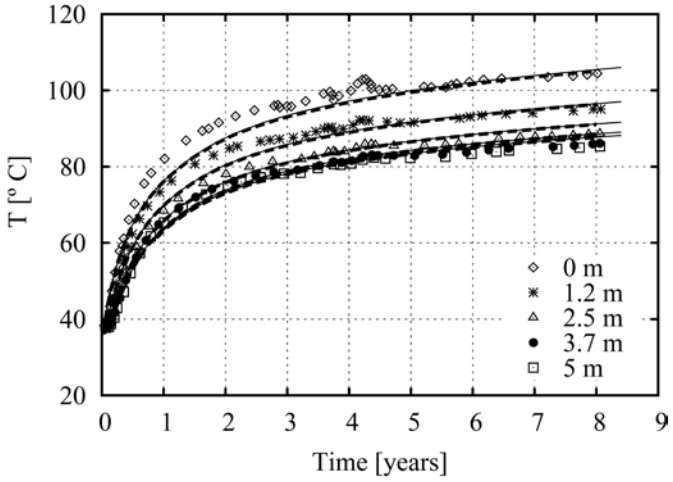

Figure 2-9. TSDE test: temperature evolution within the pillar between the two test drifts (section A). Points represent measurements, solid lines correspond to TOUGH-FLAC and dashed lines correspond to FLAC-TOUGH.

From the figures shown, we conclude that the temperature evolution and distribution during the TSDE experiment (heated and cold areas) is very well captured by TOUGH-FLAC and FLAC-TOUGH. Also, available formulations for the evolution of the backfill thermal conductivity yield very similar results, with only some differences in the temperature at the heater cask.

2.5.3 Heating phase: drift closure, backfill porosity and rock deformation

The drift closure over time is displayed in Figure 2-10, for the heated (section G1) and non-heated (section E2) areas. Drift closure is calculated from horizontal and vertical convergence data. Both the open drift and heating phases of the experiment are included in the plot. As the figure shows, the closure rate in the heated area increased significantly (factor of about 12) once heating started. High rates lasted about three months. On the other hand, the closure rate did not change noticeably in the non-heated area when the heaters were turned on. In the heated area, the closure rate decreases progressively over time due to the compaction of the backfill. Indeed, as compaction moves forward, the backfill densifies, stiffens, and provides increased mechanical support against the drift walls, thereby reducing the drift closure rate. On the other hand, in the non-heated area the drift closure rate changes smoothly, and during the last five years of heating, the vertical and horizontal closure rates are respectively 0.26-0.5%/year and 0.26-0.3%/year (values close to those of the open drift phase). In the heated area, closure rates stabilize at 0.5%/year (vertical) and 0.4%/year (horizontal). As the figure shows, numerical predictions obtained by the two simulators are very similar. Moreover, they fall within the range of experimental measurements. We note that in agreement with experimental evidence from the post-test dismantling phase (Bechthold et al., 1999), vertical closure rates are higher on the pillar side of the drift. Also, due to the flat floor and the arch-shaped roof, vertical displacement is higher at the floor (uplift).

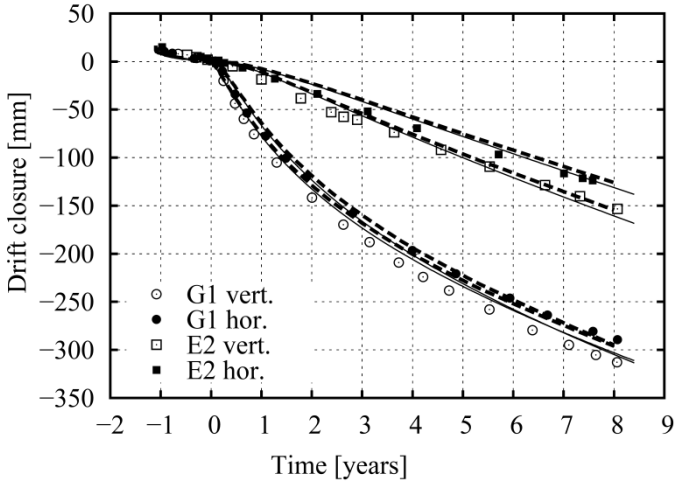

Figure 2-10. TSDE test: drift closure in the heated area (section G1) and in the non-heated area (section E2). The start of the heating phase is set as a reference time (t=0), and also as a reference for drift closure (i.e., during the open drift phase, the drifts are closing). Points represent measurements, solid lines correspond to TOUGH-FLAC and dashed lines correspond to FLAC-TOUGH.

The numerical closure rate displayed in Figure 2-10 has been obtained after the recalibration of three parameters that control the stationary creep of the natural salt host rock (recall that the transient creep finishes during the open drift phase): two of these parameters control the effect of the von Mises equivalent stress on Maxwell viscosity, and the other controls the effect of temperature on that viscosity. These two effects are strongly nonlinear, and therefore results are very sensitive to them. In addition, the three parameters adjusted are very difficult to measure at laboratory-scale, because they require very small deviatoric stresses, which translate into very small strain rates (about 10^{-10} s^{-1}), and therefore, exceedingly long test durations. Consequently, modeling a large-scale, monitored experiment is a useful means for their determination.

Figure 2-11 shows the evolution of backfill porosity in the same sections as displayed in Figure 1-10. In fact, since backfill porosity was not directly measured during the test, the experimental values displayed in Figure 2-11 were recalculated from experimental drift closure measurements (Bechthold et al., 1999). On the one hand, this yields an average porosity within a cross-section; on the other hand, the comparison between experimental data and numerical results for porosity is only approximate. Indeed, high temperature gradients develop within the backfill (see Figure 2-5 and Figure 2-7), and drift closure rates are not uniform; as a result, significant porosity gradients within the backfill are likely, even within a cross-section (heterogeneous compaction) (Bechthold et al., 2004). As the figure shows, during the heating period the average porosity reduced from 35% to 24-25.5% in the heated area, and from 35% to 30-32% in the non-heated area. Therefore, the compaction of the backfill was partial during the test. Using the porosities displayed, maximum values of thermal conductivity reached after 8 years were around 1.5 $Wm^{-1}K^{-1}$ according to Eq. (2.3) (the initial thermal conductivity was 0.8 $Wm^{-1}K^{-1}$).

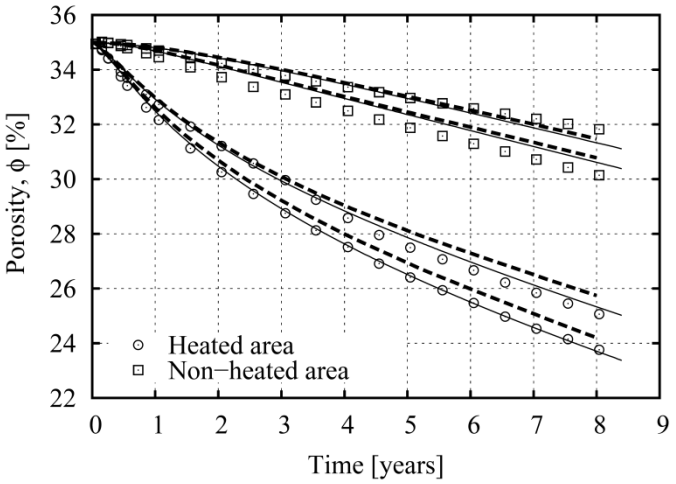

Figure 2-11. TSDE test: backfill porosity in the heated area (section G1) and in the non-heated area (section E2). Points represent measurements, solid lines correspond to TOUGH-FLAC and dashed lines correspond to FLAC-TOUGH.

Finally, Figure 2-12 shows the horizontal displacements beside the heated drifts (extensometer data), in the pillar side of the drift (section A). Experimental data are available until the extensometers failed (after about 7 years of heating). The numerical predictions obtained by TOUGH-FLAC and FLAC-TOUGH are very similar, and they match quite well the experimental data.

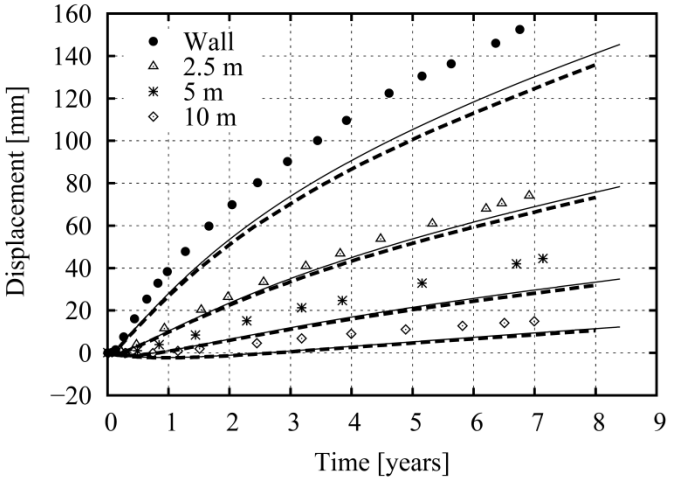

Figure 2-12. TSDE test: horizontal displacement at the wall. Points represent measurements, solid lines correspond to TOUGH-FLAC and dashed lines correspond to FLAC-TOUGH.

From Figure 2-10 and Figure 2-12, we conclude that drift closure and rock deformation trends are quite well reproduced using the two simulators used in this study.

2.5.4 Parameter calibration for backfill

Backfill compaction at relevant conditions for heat-generating nuclear waste is under investigation (Broome et al., 2014; Kröhn et al., 2012). As explained in section 2.2, we model crushed salt time-dependent compaction using a modified version of the *cwipp* constitutive model, with a parameter set adapted from previous studies (DBE 2001; Itasca, 2012). Using this parameter set, numerical predictions of the backfill stress evolution during the TSDE experiment were not satisfactory, since they yielded very small values as compared to the experimental ones. Experimental backfill stress was measured using hydraulic pressure cells, both in the hot and cold areas of the drifts (Bechthold et al., 1999).

In an attempt to reproduce the measured backfill stress more accurately, we performed a parameter estimation using the inverse modeling theory.

Using the inverse modeling framework, it is possible to estimate a parameter set that best matches available data regarding the response of a system (Finsterle, 2007). In the current case, we seek to calibrate the parameters of the *cwipp* model (compaction part) that best match measured backfill pressure, in the hot and cold areas of the test drifts. The compaction strain rate tensor, $\dot{\varepsilon}_{ij}^{vc}$ in Eq. (2.5), reads

$$\dot{\varepsilon}_{ij}^{vc} = \dot{\varepsilon}^{vc}\left(\frac{\delta_{ij}}{3} - \frac{s_{ik}\delta_{kj}}{\sigma_{VM}}\right) \tag{2.7}$$

where δ_{ij} [-] is the Kronecker delta, s_{ik} [MPa] is the deviatoric stress tensor and σ_{VM} [MPa] is von Mises equivalent stress. The compaction strain rate is given by

$$\dot{\varepsilon}^{vc} = \frac{B_0}{\rho}\left[1 - \exp\left(-B_1\sigma_{ll}^{'}\right)\right]\exp\left(B_2\rho\right) \tag{2.8}$$

where B_0 [kg·m^{-3}·s^{-1}], B_1 [MPa^{-1}] and B_2 [m^3·kg^{-1}] are model parameters, $\sigma_{ll}^{'}$ [MPa] is the mean effective stress and ρ [kg·m^{-3}] is the drained density (Itasca, 2012). As density increases during compaction, the elastic parameters (bulk, *K*, and shear, *G*, moduli) evolve according to a nonlinear empirical expression of the form

$$a = a_{\text{salt}}\exp\left(a_1\left[\rho - \rho_{\text{salt}}\right]\right) \tag{2.9}$$

where $a=\{K,G\}$ [MPa], $a_{salt}=\{K_{salt},G_{salt}\}$ [MPa] are the elastic constants of the natural salt and ρ_{salt} [kg·m^{-3}] is the drained density of the natural salt. Parameter a_1 [kg^{-1}·m^3] is obtained from the condition that the moduli take their initial values at the initial value of density (Itasca, 2012).

In order to perform several runs in a relatively short time (using a forward finite difference approximation, an inversion requires p+1 forward runs per iteration, where p is the number of parameters to be estimated [four in our case]), we decided to use a reduced model. Our reduced model comprises the drift only (crushed salt and heaters), and we applied the measured drift closure data (Figure 2-10) as a boundary condition along the drift, fixing the displacement

normal to cross-sections Y=0 m and Y=38.5 m. We used different closure rates for the hot and cold areas.

The inversions were performed using iTOUGH2 density (Finsterle, 2007), linked to the PEST protocol (Doherty, 2008). Using this protocol, the algorithms implemented in iTOUGH2 (originally written to perform parameter estimation on TOUGH2 parameters) are model-independent and can be applied to non-TOUGH2 models, as in our case (we seek to estimate mechanical compaction parameters). Figure 2-13 shows the workflow of iTOUGH2-PEST. More details about the use and theory of iTOUGH2-PEST can be found in Finsterle and Zhang (2011).

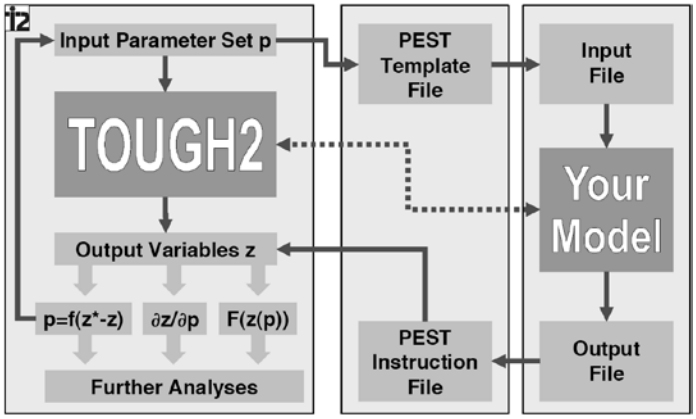

Figure 2-13. TSDE test: architecture of iTOUGH2 linked to the PEST protocol.

Figure 2-14 shows our reduced model (left), including boundary conditions (drift closure rates in the hot and cold areas), and the results of the inversion (right), in terms of experimental backfill pressure and numerical predictions using the estimated parameter set.

The parameters estimated are B_0, B_1 and B_2 of the *cwipp* model (Itasca, 2012), and also the initial Young's modulus of the crushed salt, E_0. Table 2-2 shows the initial values of these four parameters (i.e., before performing the inversion), and the best parameter set found through the inversion with iTOUGH2-PEST.

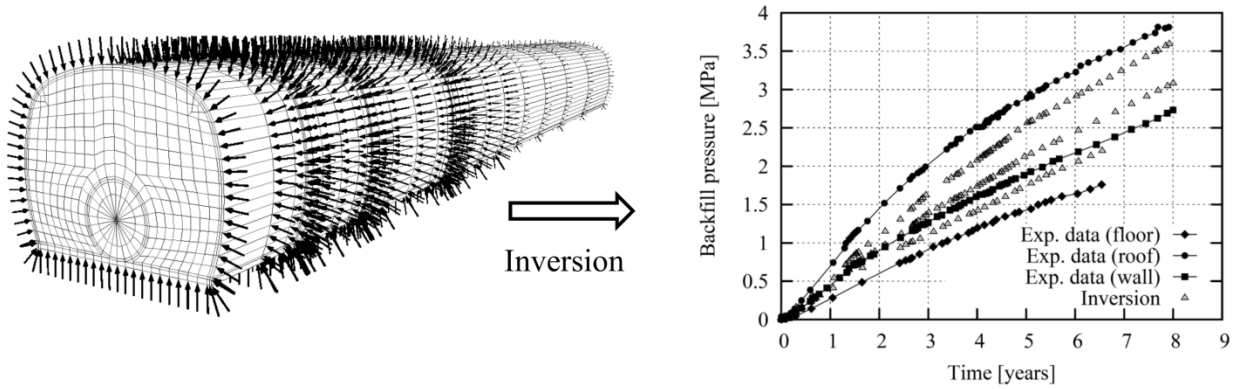

Figure 2-14. TSDE test: reduced model used in the inversion (left) and results (right).

Table 2-2. Parameter sets used to model compaction, before and after the inversion.

Parameter [unit]	Before inversion	After inversion
B_0 [kg·m^{-3}·s^{-1}]	8.6e8	4.6e8
B_1 [MPa^{-1}]	0.195	2
B_2 [m^3·kg^{-1}]	-0.0172	-0.0246
E_0 [MPa]	182	10

Figure 2-15 shows experimental and predicted backfill pressure (using the new parameter set), both in the hot (section D1) and the cold (section E1) areas. Initial stress values are atmospheric. The predictions offered by the two simulators are in quite good agreement between them, and maximum differences between predictions and measurements are about 0.8 MPa (roof in section D1).

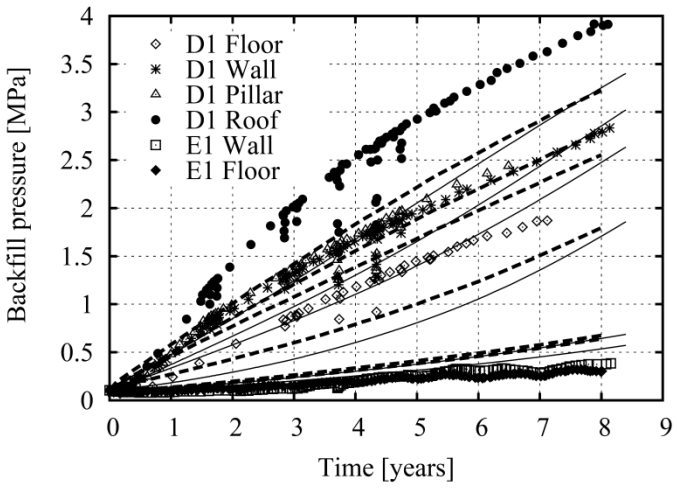

Figure 2-15. TSDE test: backfill stress increase in the heated area (section D1) and in the non-heated area (section E1). In the non-heated area, the oscillations in the experimental data are due to seasonal changes. Points represent measurements, solid lines correspond to TOUGH-FLAC and dashed lines correspond to FLAC-TOUGH.

It is believed that a better match would be very difficult to obtain, for several reasons. First, backfill compaction is very heterogeneous. Second, during the inversion two drift closure rates were applied at the drift contour (hot and cold areas), but the real rates likely change progressively over the drift length, although their evolution is not known, and may be affected by local effects such as the presence of a heater cask. Third, available drift closure and backfill pressure data were not measured in the same cross-sections, which introduces additional uncertainty to the parameter estimation. Fourth, different parameter sets may lead to a similar prediction during the inversion, depending on the topology of the objective function (Finsterle, 2007).

Although the match between experimental data and numerical predictions is now more satisfactory than initially, the parameter estimation does not inform about the physical meaning of the parameters or their suitability for other scenarios. For that purpose, we have attempted to model one oedometer test performed on crushed salt cored from one of the TSDE drifts (dismantling phase). The test was conducted on a cylindrical sample (height of 140 mm and diameter of 280 mm), at a constant temperature of 50 °C. The initial compaction rate applied was 6.9×10^{-8} s^{-1}. This rate was increased to 6.9×10^{-7} s^{-1} when the porosity was about 19%. Figure 2-16 compares experimental data with our numerical predictions. As the figure shows, there are significant discrepancies, which could be due to the need to model compaction as a function of temperature (in the *cwipp* model, compaction is temperature-independent). Another possibility is that the total strain rate should take part in the definition of the compaction strain rate. Experimental evidence at relevant conditions and more modeling exercises are necessary to clarify these points.

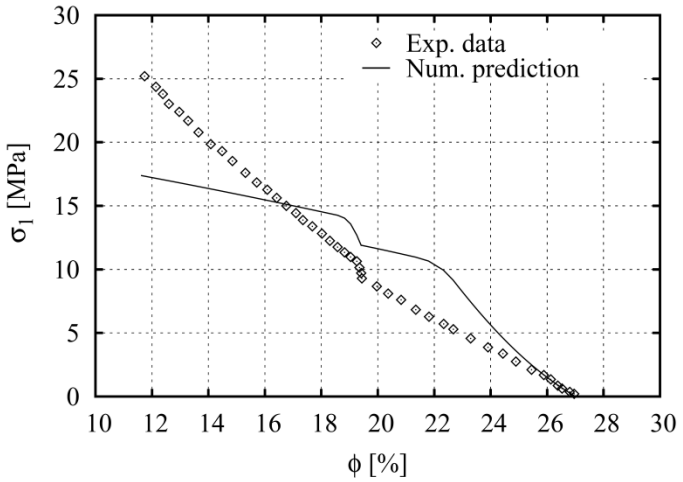

Figure 2-16. TSDE test: prediction of an oedometer test conducted on a crushed salt sample taken from one of the TSDE drifts.

3. SALT R&D

3.1 Recalculation of Generic Salt Repository in 2D

3.1.1 Introduction

In FY2014, we presented THM simulation results of a generic salt repository for heat-generating nuclear waste (Rutqvist et al., 2014). In our generic repository, the waste packages are placed parallel to the drift axis, similarly to the TSDE test. Crushed salt is used as backfill material. In the post-closure phase, our simulations were extended to 100,000 years. In addition to post-closure, we also modeled the stages of initial equilibrium, excavation and waste emplacement, and subsequent backfilling.

In FY2015, before achieving a good prediction of the TSDE experiment, we revisited our 2D model and made some improvements. The most recent results have been reported in (Blanco-Martín et al., 2015a, b). We explain the main improvements here, and summarize the latest results.

In FY2016, we intend to analyze this 2D case using the parameter set for the *cwipp* model found through the inversions performed for the TSDE test, described in the previous Section. In addition, for the natural salt we intend to use the three parameters that were recalibrated during the TSDE modeling activities (Maxwell viscosity, see previous Section).

3.1.2 Summary of improvements

We have re-run our simulations using parameters that are more relevant to natural salt (Camphouse et al., 2012; Jové-Colón et al., 2012). These include changes in the residual gas and liquid saturations in the relative permeability curves, as well as the use of different capillary pressure curves, adapted from (Olivella et al., 2011). We would like to highlight that it is extremely difficult to find capillary pressure data for natural salt (Kuhlman, 2014).

An important improvement is related to fluid infiltration. If fluid infiltration (or permeation) occurs (because the pore pressure exceeds locally the least compressive principal stress), a

secondary permeability develops. Due to numerical instabilities, we were limiting this maximum secondary permeability to about 10^{-20} m^2. As a result, maximum pore pressures predicted were about 25 MPa.

During FY2015, we have overcome those numerical instabilities, and now the maximum pore pressure predicted in the infiltration scenario does not exceed 15-16 MPa. We think these results are much more realistic. An overview is presented below.

3.1.3 Model description

Figure 3-1 shows the model geometry and main dimensions, with an enlarged view of the area near the drift (same model as in FY2014). The model extends 1200 m in the vertical direction and starts at the ground surface. The repository is located in the middle of a 400 m thick salt layer, at a depth of 600 m. Two 400 m thick sandstone layers confine the rock salt layer. The drifts are 4.5 m wide and 3.5 m high. The cylindrical metallic canisters are 5.5 m long, have a diameter of 1.6 m and are separated by 3 m along the drift axis. At this stage, we consider a two-dimensional plane-strain assumption. Symmetry allows modeling just half of one drift. In the *X* direction, the drifts are 50 m apart.

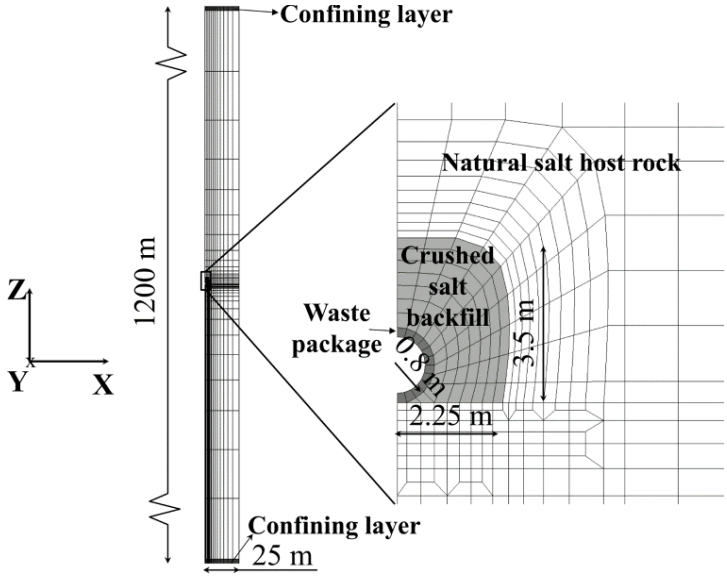

Figure 3-1. Generic Salt Repository in 2D: geometry of the generic salt repository studied and detailed view of the drift area.

Along with the mechanical response, two-phase flow of water and air (by advection and diffusion) and heat flow (by conduction and convection) are modelled. TOUGH2 Equation-Of-State (EOS) module 4 is used (Pruess et al., 2011). This module provides a capability for vapor pressure lowering, which allows a liquid phase to exist when the vapor partial pressure and the gas phase pressure are lower than the saturation pressure (due to phase adsorption and capillary effects). Vapor pressure lowering is modelled via Kelvin's equation (Pruess et al., 2011).

As in previous years, the heat released by each waste package is consistent with the expected nuclear waste characteristics in the US Department of Energy Used Fuel Disposition Campaign (Carter et al., 2011). It is assumed that each waste package comprises ten pressurized water reactor (PWR) assemblies and that the packages are emplaced underground after 20 years of interim storage. The heat load evolution after emplacement is displayed in Figure 3-2 (note that the time is reset to zero when the waste packages are emplaced underground).

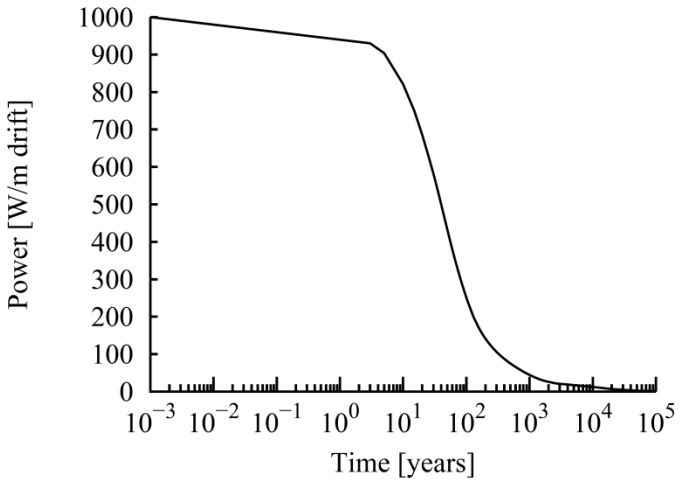

Figure 3-2. Generic Salt Repository in 2D: heat load per meter of drift for a waste package containing 10 PWR assemblies, assuming underground emplacement after 20 years of interim storage.

Table 3-1 lists parameters used for the crushed salt, the host rock and the confining layers. Some of these parameters have been adopted from previous research (Bechthold et al., 2004; Camphouse et al., 2012; Jové-Colón et al., 2012; Olivella et al., 2011). We highlight that, in the absence of sufficient experimental data on capillary effects in natural halite, we have used an extrapolation of capillary pressure data corresponding to granular salt (Olivella et al., 2011), using a Leverett factor (Cinar et al., 2006; Leverett, 1941). The van Genuchten function (van Genuchten, 1980) is used for all materials. Temperature and hysteresis effects on water retention are neglected.

Table 3-1. Mechanical and flow properties of the crushed salt, natural salt and confining layers.

Property [unit]	Crushed salt	Rock salt	Confining rock
Grain density, ρ [kg·m^{-3}]	2200	2200	2600
K [MPa]	150[a]	16,650[b]	37,900
G [MPa]	70[a]	7690[b]	19,500
α_T [K^{-1}]	$4\cdot10^{-5}$	$4\cdot10^{-5}$	10^{-5}
α [-]	1[a]	0.003[b]	1
Relative permeability functions	Corey	Corey	Van Genuchten (liquid), Corey (gas)
Residual liquid saturation, S_{lr} [-]	0.1	0.1	0.02
Residual gas saturation, S_{gr} [-]	0	0	0.01
Van Genuchten's λ [-]	0.6	0.6	0.6
Van Genuchten's P_0 [MPa]	0.0004[c]	5.7[c]	3.6
Van Genuchten's S_{lr} [-]	0.01	0.01	0.01

[a]: non-constant value
[b]: values are damage- and healing- dependent
[c]: non-constant value

From a mechanical viewpoint, the waste package and the confining layers are assumed to behave elastically. The *Lux/Wolters* model parameters used for the host rock have been obtained from the interpretation of experimental results (Lerche, 2012). Regarding the *cwipp* model for the crushed salt, the values used have been adapted from available experimental data (DBE, 2001; Itasca, 2012). Since experimental data for porosities smaller than 5-10% are scarce, some uncertainties exist about the validity of the parameters used.

The molecular diffusion coefficients depend on pressure and temperature (Vargaftik, 1975; Walker et al., 1981). Tortuosity effects are accounted for using the Millington-Quirk model (1961). Initial flow parameters are listed in Table 3-2. The absolute permeability k is assumed isotropic for every material.

A geothermal gradient of 0.03 K·m^{-1} is initially applied to the model. This corresponds to about 28 ºC at the repository level assuming a ground surface temperature of 10 ºC. The initial mechanical condition is isotropic stress, equal to the lithostatic stress magnitude (overburden); this corresponds to about -14 MPa at Z=-600 m (compression is negative). For the calculation of the pore pressure, we assume that the water table is at the ground surface. Regarding the fluid inclusions at the boundaries of natural salt crystals, we assume an initial liquid saturation of 100%.

Table 3-2. Initial flow parameters of the crushed salt, natural salt, and confining layers.

Parameter [unit]	Crushed salt	Rock salt	Confining rock
S_l [-]	0.015	1	1
ϕ [-]	30 %	0.2 %	12 %
k [m^2]	$3\cdot10^{-13}$	10^{-22}	10^{-17a}
C [J·kg^{-1}·K^{-1}]	860	860	900[a]
λ [W·m^{-1}·K^{-1}]	0.9	4	1.8[a]

[a]: constant values

Prior to the THM run, the excavation, subsequent emplacement of the waste packages and drift back-filling are modelled in FLAC^{3D} to account for the induced stress redistribution and possible changes in the pore pressure. The pore pressure obtained after the excavation is exported to TOUGH2, so that the initial conditions of the THM run are the same in the two codes (the coupled THM simulation covers the post-closure phase of the repository, once the heat-generating waste packages are emplaced and the drifts backfilled). Note that the initial pore pressure within the backfill and the waste package is set to 0.1 MPa (atmospheric pressure).

In TOUGH2, Dirichlet boundary conditions are assigned to the top and bottom grid blocks, so that their thermodynamic state remains unchanged. Owing to symmetry, the lateral surfaces of the model are no-flow boundaries. In FLAC^{3D}, the horizontal displacement is blocked in planes X=0 and X=25 m, as well as the vertical displacement in plane Z=-1200 m. Gravitational effects are considered in both codes.

3.1.4 Main results

Figure 3-3 displays the temperature evolution at different positions in the repository over the simulated 100 000 years of post-closure phase. This evolution is very similar to that obtained during FY2014. The temperature at the waste package surface peaks slightly below 200 °C after about one year. The nearby crushed salt and host rock also show an initial temperature peak. This local peak is due to the low thermal conductivity of the backfill before significant compaction takes place. After 25 years, a temperature peak of about 160 ºC is obtained in the drift area. The temperature 25 m away from the drift peaks at about 108 ºC after 80 years, reflecting progressive heat propagation through the natural salt host rock.

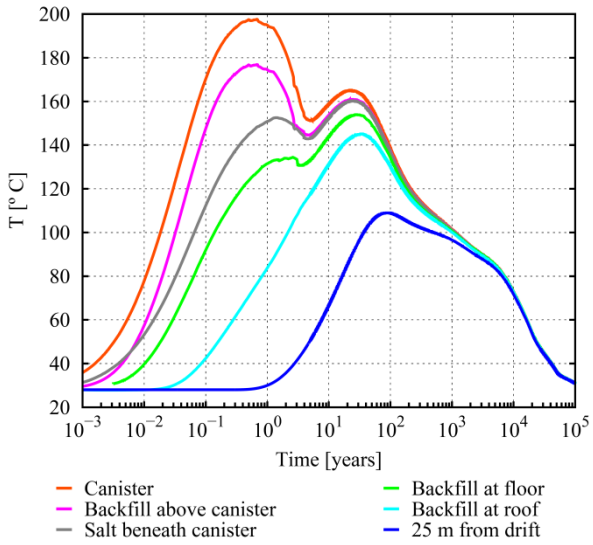

Figure 3-3. Generic Salt Repository in 2D: temperature evolution during the post-closure phase, at six locations within the repository.

Crushed salt reconsolidation occurs in a similar fashion as well (see Figure 2-4). The predicted duration of the reconsolidation process may be too short and we highlight that it is uncertain for

now. Therefore, these results are not conclusive. As more reconsolidation data at relevant loading conditions and temperatures become available, these predictions may change.

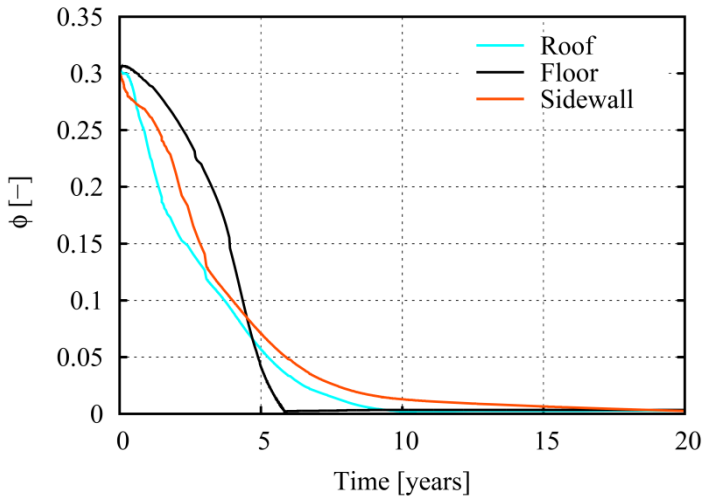

Figure 3-4. Generic Salt Repository in 2D: porosity evolution within the crushed salt, during the first 20 years of post-closure phase.

Figure 3-5 (left) shows the evolution of pore pressure and Figure 3-5 (right) displays the evolution of liquid saturation at five different positions in the repository: three locations in the host rock and two locations in the crushed salt. As the backfill liquid saturation increases steeply just before 10 years, the pore pressure increases in a similar fashion. Additionally, as the backfill saturation increases the pore pressure is the same at the five locations monitored. The pore pressure peaks below 16 MPa. Indeed, pore pressure cannot increase much above the infiltration criterion because infiltration will work against further pore pressure increase, and it cannot decrease below the infiltration criterion because the infiltration-induced grain boundary openings and/or micro-fractures will close again, triggering a new pore pressure increase, which will result in infiltration. In the current scenario, the main cause to fluid permeation is the thermal pressurization of the liquid phase induced by the time-dependent release of decay heat from the waste packages. As the heat load and temperature decrease over time (see Figure 3-2 and Figure 3-3) pore pressure and infiltration reduce progressively (see left-hand side plot in Figure 3-5), and the initial permeability of the host rock is restored.

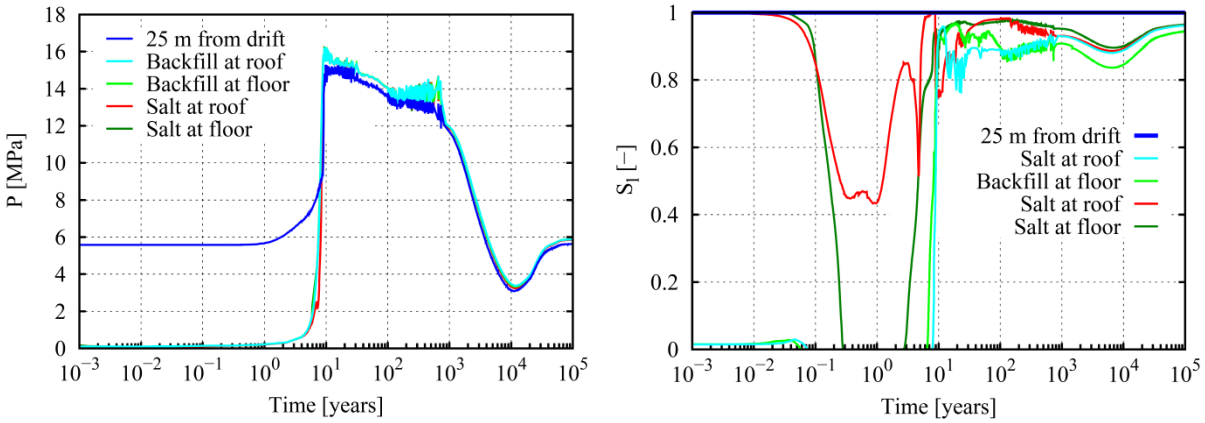

Figure 3-5. Generic Salt Repository in 2D: pore pressure evolution (left) and liquid saturation evolution (right) at different locations during the post-closure phase.

The analysis of the results shows that fluid permeation into the rock starts after 6 years at a location 8 m away from the drift along the *X* axis. Permeation does not start in the drift area because the pore pressure is smaller in this zone due to the partial desaturation of the near-field host rock in the first years of the post-closure phase, see Figure 3-5 (the first temperature peak and the porosity increase trigger this partial desaturation). After 10-20 years, the pressure is uniform in the backfill and near-field host rock and pressure-driven fluid infiltration occurs. The area that undergoes infiltration is significantly larger than the area affected by thermo-mechanical damage (EDZ); it extends at the repository level along the *X* and *Z* axes as pressure increases (thermal pressurization), but it does not reach the confining layers (the extension along the Z axis is about 100 m above and below the drift). Finally, we note that the reconsolidated backfill also undergoes infiltration if the infiltration criterion is met.

3.2 Modeling Coupled Processes accounting for halite dissolution and precipitation

3.2.1 Introduction

In this part, we describe the main enhancements to TOUGH-FLAC during FY15 for the modeling of coupled processes in saliferous media within the context of disposal of heat-generating nuclear waste.

In previous reports (Rutqvist et al., 2013, 2014), we presented the modifications introduced to account for large strains and creep processes. Moreover, in FY14 we improved the efficiency of the simulations by reducing the computational time by a factor of 3 to 4, i.e. 3 to 4 times faster. We also linked TOUGH-FLAC to the open source code Voro++ to compute Voronoi partitions corresponding to the current geomechanics deformed mesh. These enhancements have been recently published (Blanco-Martín 2015a,b).

In FY15, the enhancements are mostly related to the flow sub-problem. In particular, now we not only account for the flow of water and air, but also for the flow of brine. Indeed, we now consider three components in the flow sub-problem: water, air, and halite. The liquid phase is not composed of water with dissolved air, but by brine (solution of halite in water) with dissolved air. Halite (sodium chloride, NaCl) is very soluble in water, and solubility increases with

temperature. However, if the mass fraction of halite in the liquid phase exceeds the solubility limit (which is a function of temperature), precipitation of solid halite will occur. Conversely, dissolution of solid salt will occur if the mass fraction of halite in the liquid phase is lower than the solubility limit at the current temperature. Halite solubility constraints introduce a new phase into the flow sub-problem, so that in addition to the gas and liquid phases, a solid phase is also possible. As shown in the literature, the presence of a solid phase affects porosity and permeability (Olivella et al., 1996, 2011; Rege and Fogler, 1989), and therefore may have an impact on the flow barrier role of the host rock and the backfill. To evaluate these impacts, we have performed coupled simulations of a generic salt repository accounting for these effects, and we have compared the results with simulations in which halite solubility constraints are neglected.

In this section, we first describe the thermo-dynamical properties of brine and halite, and how they are considered in TOUGH2. Then, we describe the provisions needed to account for a solid phase in the computation of mass and heat flows. Later, we present the enhancements of the TOUGH-FLAC simulator to account for salt dissolution and precipitation effects. In terms of simulations, we first benchmark TOUGH2 and TOUGH-FLAC against other codes (CODE_BRIGHT in particular) and experimental data. Finally, we present the results obtained so far in our generic salt repository (2D). This generic repository is the same as in previous reports and Section 3.1. As usual, we include the phases of excavation, waste emplacement, backfilling and post-closure (100,000 years).

We highlight that this research in very innovative. Lately, research has been undertaken regarding the modeling of the impacts of halite dissolution and precipitation in the context of underground disposal of nuclear waste in rock salt, but without accounting for mechanical processes (Jordan et al., 2015; Stauffer et al., 2013, 2014). Here, we consider sequential coupling of thermal, hydraulic and mechanical processes, both in the crushed salt and in the natural salt host rock.

3.2.2 Thermo-dynamical properties of halite and brine

Solid halite (NaCl) is very soluble in water. Dissolution of halite in water results in brine. Halite is also soluble in steam; however, the mass fraction of halite in salt-saturated steam is orders of magnitude smaller than the mass fraction of halite in saturated brine (Palliser and McKibbin, 1998). Figure 3-6 shows the solubility of halite in brine and water vapor as a function of temperature, computed using recent models developed by Driesner and Heinrich (2007) for brine, and by Palliser and McKibbin (1998) for steam. These are the models used in our simulations.

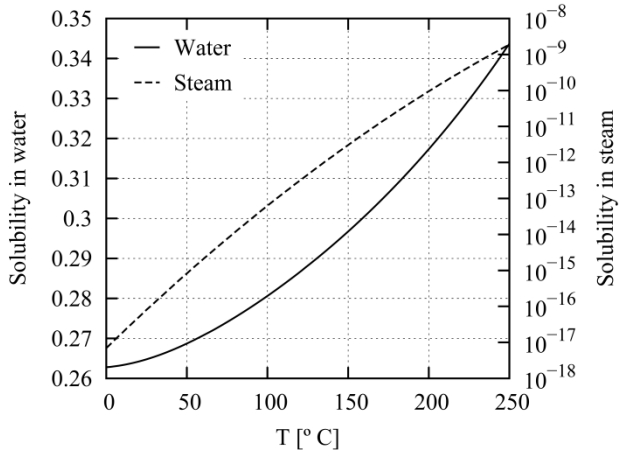

Figure 3-6. Temperature-dependent solubility of halite (NaCl) in brine (left *y* axis) (Driesner and Heinrich. 2007) and in steam (right *y* axis) (Palliser and McKibbin, 1998).

We note that the solubility dependence on pressure is negligible for temperatures smaller than 400 °C (Driesner, 2007). Since the temperatures of interest in our research are much smaller than this value, we neglect the pressure dependence of halite solubility.

The density of solid halite decreases with the increase of temperature and increases if pressure increases. We use a model by Driesner (2007) to compute the density of solid halite. The values provided by this model for the temperatures and pressures relevant to our research are shown in Figure 3-7.

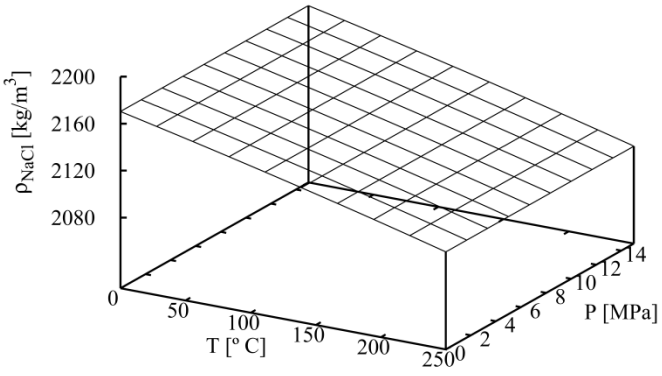

Figure 3-7. Density of solid halite (NaCl) as a function of pressure and temperature (Driesner, 2007).

The specific enthalpy of halite is also a function of pressure and temperature. As with density, we use a recent correlation developed by Driesner (2007). Details of this correlation can also be found in Battistelli (2012).Molecular diffusion of halite in brine is temperature-dependent. We use a diffusion coefficient described in Olivella et al (1996):

$$d_l^{NaCl} = (1.1\text{E}-4)\exp(\frac{-24530}{R(273.15+T)}) \qquad (3.1)$$

Where d_l^{NaCl} is the diffusion coefficient [m^2/s], T is temperature [°C] and R=8.314 J/K·mol. Molecular diffusion of water in air is modeled using the same model as in previous reports (Vargaftik, 1975; Walker et al., 1981). In that model, vapor diffusion is temperature and pressure dependent.

As for brine, its density and specific enthalpy are also functions of pressure and temperature. We use approaches developed by Andersen et al. (1992) and Phillips et al. (1981), respectively. Brine density increases with halite concentration and with pressure, and decreases with temperature.

3.2.3 Particular provisions for water-air-halite mixtures

As it was explained before, when halite is accounted for to study the fate and transport of mass and heat flows in porous media, a third component (halite) has to be considered. Therefore, there is an additional equation per grid-block. Moreover, there is a third phase (solid). The solid phase is composed solely by halite. From the flow perspective the solid phase is immobile, i.e., there is no mass transport of solid halite. This particularity introduces the concept of an effective porosity, defined as the pore space occupied by the liquid and the gas phases (i.e., the mobile phases). On the other hand, the total porosity, defined as the pore volume divided by the total volume of one grid-block, includes the solid phase. The relationship between the effective and the total porosity reads

$$\phi_{eff} = \phi(1 - S_s) \qquad (3.2)$$

where ϕ_{eff} [-] is the effective porosity, ϕ [-] is the total porosity and S_s [-] is the solid saturation. Flow properties that depend on saturation, such as capillary pressure and relative permeability of the mobile phases, should be calculated on the basis of the effective porosity.

Phase changes are affected by the presence of dissolved halite. Indeed, as the concentration of NaCl in brine increases, the vapor pressure of the solution decreases (Battistelli et al., 1997). Additionally, Henry's constant increases, yielding higher dissolved air pressures (*salting out* effect, or reduction of air solubility with increasing NaCl in the liquid phase). At a given temperature, viscosity of vapor-saturated brine increases with the concentration of halite (Battistelli et al., 1997).

The Equation-Of-State (EOS) module of TOUGH2 EWASG (WAter, Salt, Gas) effectively accounts for the thermo-physical properties of fluids of variable salinity (Battistelli et al., 1993). In previous investigations, we were using EOS3 and EOS4 (water-air mixtures). EWASG was developed for the modeling of hydrothermal systems containing salt and a non-condensable gas (NCG), such as air. The standard version of this EOS fluid property module has been recently improved to overcome some limitations (Battistelli, 2012); some of these limitations are related to the correlations used for brine and halite, which were derived from different sources (with a potential risk for limited internal coherence). Additionally, the effects of NCG were evaluated

with an approach limited to low partial pressures. The correlations for halite and brine described in this Section correspond to the newest version of EWASG.

3.2.4 Enhancements of TOUGH-FLAC to account for halite solubility constraints

As in previous related studies (Blanco-Martín et al., 2015a,b; Rutqvist et al., 2013, 2014), we conduct our numerical simulations using an updated version of the TOUGH-FLAC simulator, adapted for large strains and creep processes (Blanco-Martín et al., 2015a). Given that the solid phase (precipitate) and the rock are the same substance (NaCl), we have included halite dissolution and precipitation effects by increasing the initial porosity of the materials present (natural salt, crushed salt) and by assigning a solid phase at the beginning of the simulations, so that the initial effective porosity defined in Eq. (3.2) is the target porosity for these materials. Indeed, brine within rock salt pores is saturated with halite. A particular requirement in our simulations is that the solid phase should always be present in some quantity in order for TOUGH2 (EWASG EOS) to model the correct thermo-dynamical processes and phase equilibria, accounting for salt solubility effects (i.e., in TOUGH2 no provision is given for dissolution of the non-porous space). This condition is satisfied in the simulation described in this report.

From a mechanical point of view, the solid phase within the pores is able to bear load, since it is considered to be regular rock salt. Thermal expansion effects are accounted for in a similar way in the solid phase in TOUGH2 and in the grains in FLAC^{3D}. Regarding compaction of the crushed salt, we have adapted the *cwipp* constitutive model (Callahan and DeVries, 1991; Itasca, 2012; Sjaardema and Krieg, 1987) to prevent the precipitate from compacting (i.e., only the effective porosity is subject to compaction).

The coupling structure between flow and geomechanics is the same as in previous studies (two-way sequential coupling), as well as the coupling functions used (Blanco-Martín et al., 2015a,b). In the mechanics sub-problem, we use the equivalent pore pressure to compute effective stresses (Coussy, 2004). The only difference as compared to our previous modeling efforts is that in the current case, permeability changes related to fluid infiltration and thermo-mechanically induced damage (host rock), as well as permeability changes related to compaction and fluid infiltration (crushed salt backfill) account for the presence of a solid phase in the pores. In other words, the permeability is calculated accounting for the effective porosity.

3.2.5 Benchmark of EWASG against CODE_BRIGHT and experimental data

Before addressing our target simulation, namely, the long-term modeling of coupled processes in a generic salt repository for heat-generating nuclear waste (with crushed salt backfill), we benchmark the TOUGH2 module EWASG against other codes and available experimental data. The target of this benchmark is to evaluate whether our numerical tools are able to reproduce relevant data in the context of disposal of heat-generating nuclear waste in salt rock mass. We note that in this report we only present benchmarks that involve crushed salt. We are currently working in the THM modeling of one heater test conducted in a borehole in room A at WIPP (Nowak, 1986; Nowak and McTigue, 1987). This test involves only natural salt (i.e., no crushed salt present). The results will be presented in FY2016.

3.2.5.1 Benchmark 1: synthetic experiment performed by Olivella et al. (1996) with CODE_BRIGHT

Olivella et al. (1996) modeled porosity variations within a crushed salt sample under a thermal gradient. In their synthetic experiment, the authors considered a one dimensional case. The system is closed, so that the mass remains constant. The temperature in one extremity is held constant at 82 °C, while the other extremity is held at 22 °C. The lateral surface of the sample is kept in adiabatic conditions. The temperature gradient is maintained for 347 days. The sample is assumed to be 0.5 m long. In the hot extremity, water evaporates and due to the steam concentration gradient in the gas phase, steam flows towards the cold end (diffusive transport), and it condenses, increasing liquid saturation. The different liquid saturation along the sample triggers a liquid pressure gradient, and therefore a flow of liquid water (by advection) from the cold end to the hot end of the sample. Thus, the system is governed by vapor diffusion and capillary forces. Deformation is blocked at the samples end, and mechanical effects are neglected.

As the water evaporates close to the hot end, precipitation of the dissolved halite occurs, which reduces the effective porosity. Similarly, as water condenses far from the hot end, dissolution of the solid halite takes place, which increases the effective porosity. Modeling porosity changes is an important aspect of this numerical exercise.

Figure 2-8 shows the comparison between CODE_BRIGHT and EWASG results, in terms of effective porosity along the sample at five different moments. As the figure shows, EWASG results are quite close to those obtained by Olivella et al. (1996) with CODE_BRIGHT. We note that numerical instabilities are obtained by both codes at 347 days close to the cold end, due to a strong extraction of salt at that end.

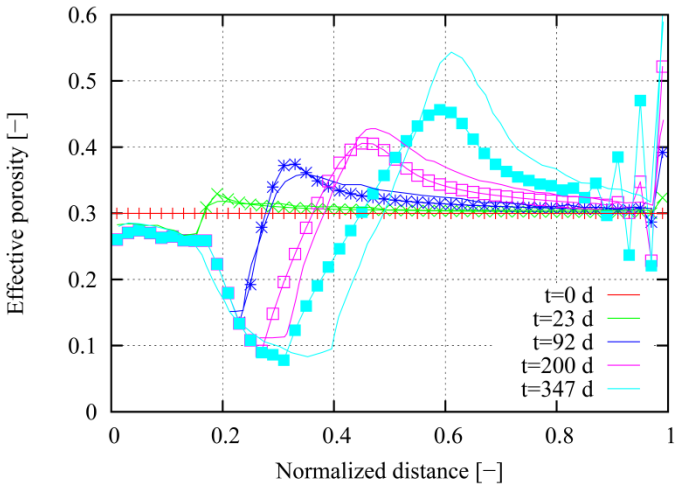

Figure 3-8. Synthetic test performed by Olivella et al. (1996): comparison between CODE_BRIGHT (solid lines) and TOUGH-EWASG (lines with points).

3.2.5.2 Benchmark 2: laboratory experiment performed by Olivella et al. (2011)

In an attempt to verify numerical predictions against experimental data, Olivella et al. (2011) performed laboratory-scale experiments that very closely represent their synthetic modeling published in 1996 (previous Section). In this case, the authors imposed a thermal gradient on several crushed salt samples. The samples (cylindrical) were 100 mm long and had a diameter of 50 mm. The crushed salt grain size was about 1-2 mm. The temperature in the hot end was fixed at 85 °C and 5 °C were imposed in the cold end. Deformations were not permitted in the sample ends, and mechanical effects are disregarded, as in Benchmark 1. The duration of each test was 65 days.

Different initial porosities were tested: 20, 30 and 40%. Similarly, three values of initial liquid saturation were investigated: 10, 30 and 40%. In this report, we focus on the "reference" case established by the authors, namely, initial porosity of 30% and initial saturation of 40%.

Figure 3-9 shows a comparison between experimental data and numerical results obtained by TOUGH2-EWASG. As the figure shows, the results are quite satisfactory. We highlight that the discrepancies observed in the cold end may be due to the fact that macro voids were observed in some samples (see Figure 3-10), due to water condensation and halite dissolution (i.e., strong extraction of salt, as predicted in Benchmark 1, see Figure 3-8); as a result, the assumption of a continuous medium may be not satisfied close to the cold end of the sample. This aspect was highlighted by Olivella et al. (2011).

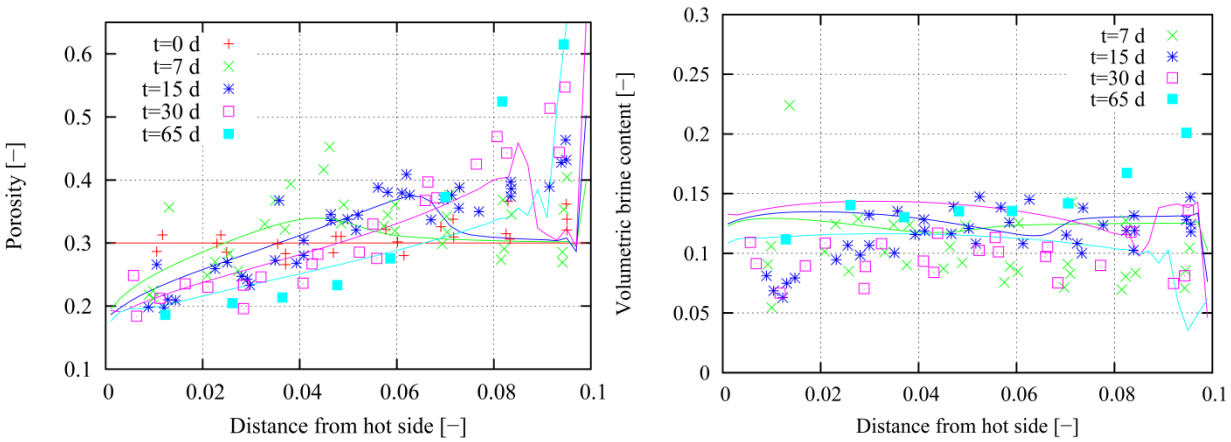

Figure 3-9. Thermal test on crushed salt performed by Olivella et al. (2011) on crushed salt: comparison between measurements (points) and TOUGH-EWASG (solid lines).

Figure 3-10. View of the cold end of one sample (test performed by Olivella et al., 2011).

3.2.5.3 Benchmark 3: laboratory experiment performed by LANL (2013).

Stauffer et al. (2013) presented results of an experiment conducted on a pile of crushed salt. In that experiment, a 125 W bulb was mostly submerged in crushed salt piled into a cone shape (height of about 31 cm). Figure 3-11 shows a view of the crushed salt and the visible part of the bulb. The duration of the test was 2 hours.

Figure 3-11. View of the experimental set-up corresponding to the thermal test on a pile of crushed salt (Stauffer et al., 2013).

The initial porosity of the crushed salt was 37.5% and initial liquid saturation was 1%. Temperatures were recorded at a frequency of 1 minute, at two distances from the bottom of the bulb: 6.35 and 15.2 cm. The authors modeled this experiment using a radial model and the

results were quite satisfactory, i.e., the measured and predicted temperature evolutions were very close to each other. Mechanical effects were disregarded.

We have modeled this experiment in a similar way as done by Stauffer et al. (2013). Due to symmetry reasons, we use an axi-symmetric model, shown in the left-hand side of Figure 3-12. The comparison between measured and predicted temperatures at 6.35 and 15.2 cm below the bulb are displayed in the right-hand side plot in the figure (for the position 6.35 cm, we have plotted predictions at 6 and 6.5 cm). As the figure shows, the results are quite satisfactory.

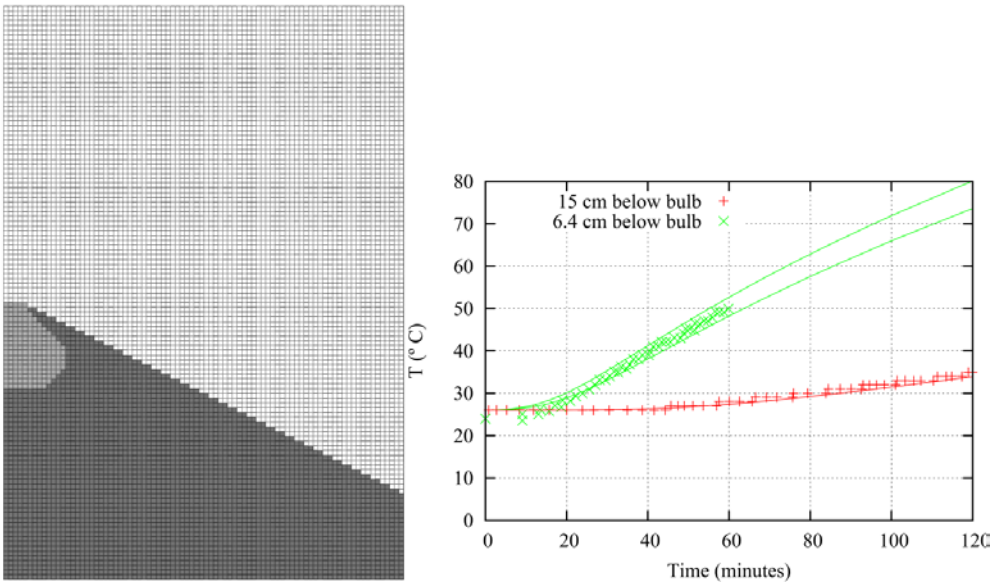

Figure 3-12. Test on a pile of crushed salt (Stauffer et al., 2013): discretization (left) and comparison between experimental data and numerical predictions (right).

3.2.6 Generic Salt Repository for heat-generating nuclear waste

3.2.6.1 Introduction

After having validated EWASG against another code (CODE_BRIGHT) and measurements, we present the results obtained for our target simulation, namely, a generic salt repository (GSR) for heat-generating nuclear waste. As a reminder, our GSR features in-drift emplacement of the waste packages and backfilling of the remaining space with crushed salt (see Section 3.1).

We highlight that in FY2016 we intend to analyze in more detail the results presented here. In particular, we intend to refine the mesh within the crushed salt to investigate the effect of the mesh size when dissolution/precipitation of halite occurs. In addition, we intend to perform these 2D simulations using the parameters (natural and crushed salts) determined during the modeling activities of the TSDE test, detailed in this report (Section 2).

3.2.6.2 Results and discussion

The scenario studied is similar to that in Section 3.1. We present the predictions that are most affected by halite solubility constraints, and we compare them to the case that neglects those constraints. In the natural salt, we set an initial solid saturation of 10% and in the crushed salt,

we set $S_{s,0}$=3% (lower value because the solid saturation will increase due to compaction). We note that the discussion below is preliminary and does not include yet a comprehensive validation based on measurement data of the physical processes.

Figure 3-13 shows the evolution of temperature at several locations in the repository during the post-closure phase (100,000 years). These results are similar to those obtained without halite solubility constraints.

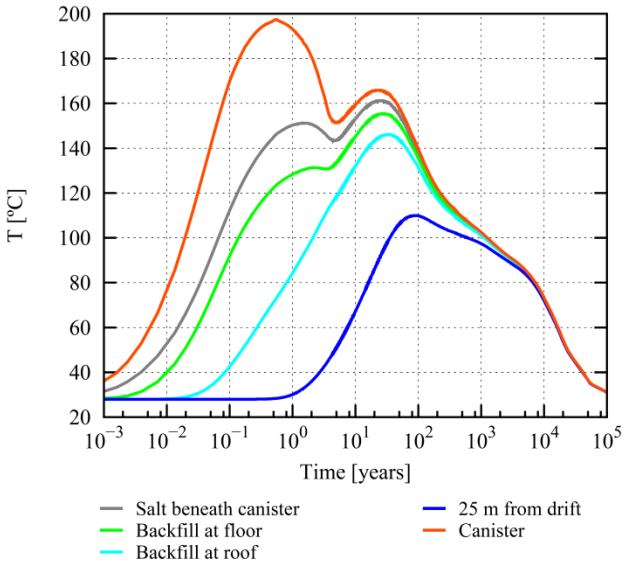

Figure 3-13. Generic Salt Repository in 2D (with solubility constraints): temperature evolution during the post-closure phase, at five locations within the repository.

As temperature increases, brine vaporization occurs within the crushed salt close to the waste package, and water condenses farther away (about 0.6-0.8 m from the waste package), where temperatures are lower. As water condenses, it dissolves halite until saturation at the corresponding temperature. Similarly, brine vaporization brings about halite precipitation. However, the changes in the quantity of solid halite are not significant within the backfill due to two main reasons: first, the initial brine saturation is very small (see Table 3-2), and second, the backfill is compacting (i.e., pore volume decrease) as a result of the drift convergence, triggered by the creep of the host rock; consequently, a substantial decrease in solid saturation is not captured. In FY2016, we intend to refine the mesh to confirm these results, and we will investigate the sensitivity of these predictions to the initial liquid saturation within the backfill.

Figure 3-14 shows the relative change in mass of solid halite within the backfill at several times (the reference time is taken when the drift is backfilled). As the figure shows, a ring of high halite dissolution develops 0.6-0.8 m away from the waste package, coinciding with the area of highest water condensation. As time goes on, temperature decreases and in parallel progressive compaction of the crushed salt occurs. Over time, some liquid phase appears again in the crushed salt close to the waste package, and halite dissolves to saturate the brine. Therefore, the mass of solid halite decreases slightly in this area as shown in the last images of Figure 2-14.

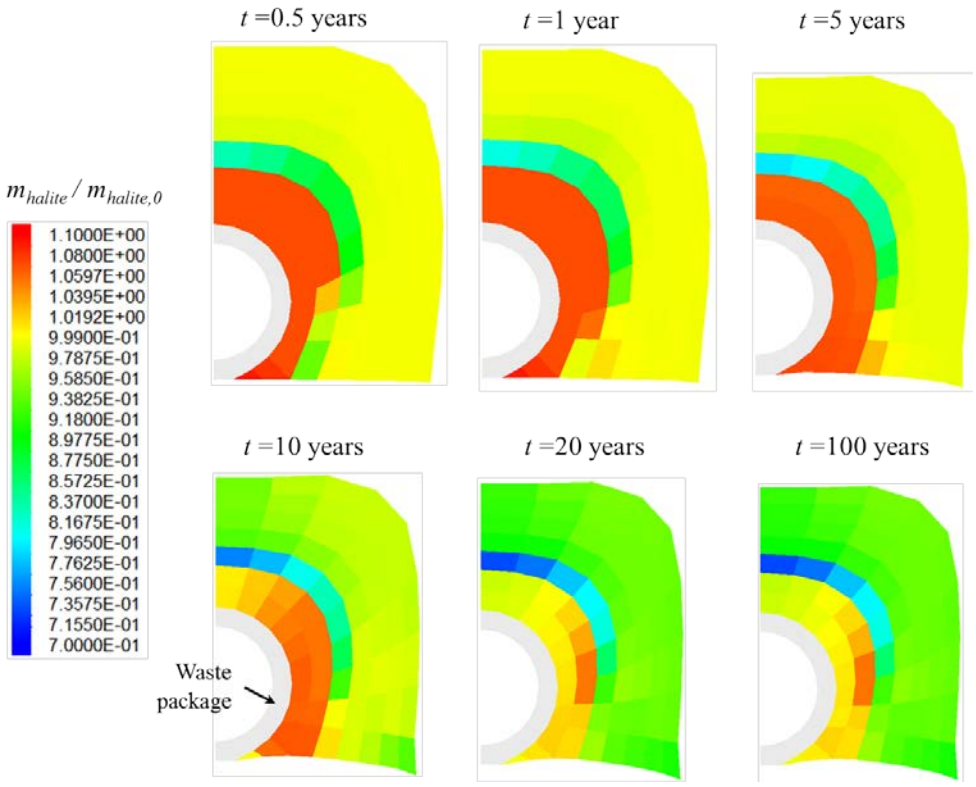

Figure 3-14. Generic Salt Repository in 2D (with solubility constraints): relative change in mass of solid halite within the backfill (reference situation is taken at drift backfilling). The change in shape is due to compaction.

As regards backfill consolidation, our preliminary results suggest that there are no major differences when halite dissolution and precipitation effects are accounted for, at least in terms of time frame and final porosities reached. The main reason for this finding is the dominating mechanical effect (compaction).We will perform additional modeling to confirm this and other initial results.

Regarding the natural salt host rock, the processes that affect its tightness during the first years develop in a similar way when halite dissolution and precipitation are considered (thermo-mechanical damage in the EDZ and activation of healing processes as the backfill reconsolidation occurs). After 7 years, the EDZ is sealed and the initial tightness of the rock restored. As temperature increases and heat propagates through the rock, halite dissolves in the brine to accommodate the solubility increase (Figure 3-6). This dissolution increases the effective porosity slightly. In this study, we have assumed that changes in effective porosity due to precipitation/dissolution affect the permeability of the medium, in agreement with previous research (Olivella et al., 1996, 2011; Rege and Fogler, 1989). As a first approach, we have assumed that the relationship between permeability and active porosity for rock salt follows a power law, similar to the relationship between porosity and permeability within the backfill during compaction (Blanco-Martín et al., 2015a). Figure 3-15 shows the secondary permeability of the host rock after 10 years in two situations: when halite solubility is accounted for or disregarded. We note that at this time, pore pressure has increased significantly in the host rock

close to the drift due to the very low permeability of the formation, its saturated conditions and the high thermal expansion coefficient of the pore fluids relative to the host rock (thermal pressurization of the pore fluids). If the pore pressure locally exceeds the minimum compressive principal stress, fluid permeation occurs and a secondary permeability develops (Wolters et al., 2012). This secondary permeability is shown in Figure 3-15. Therefore, two effects are represented in the figure: fluid permeation (present when halite solubility is accounted for or disregarded), and halite solubility.

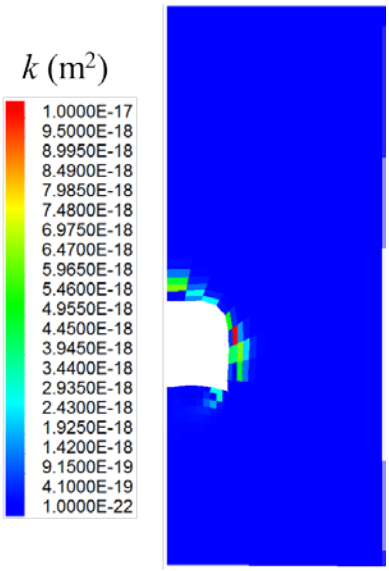

Figure 3-15. Generic Salt Repository in 2D (with solubility constraints): comparison of the area affected by secondary permeability (after 10 years) when halite solubility is accounted for (left) or disregarded (right).

Owing to solubility effects of the halite, the effective porosity is slightly higher when halite dissolution/precipitation effects are accounted for, resulting in a greater zone affected by infiltration-induced secondary permeability. However, this effect does not last long and after 30 years permeability has reduced substantially, see Figure 3-16. Indeed, as temperature decreases over time, both the pore pressure and the solubility of halite decrease, resulting in permeability decrease towards the characteristic value of undisturbed natural salt. Our results suggest that the effects of halite solubility on permeability vanish after 100-200 years.

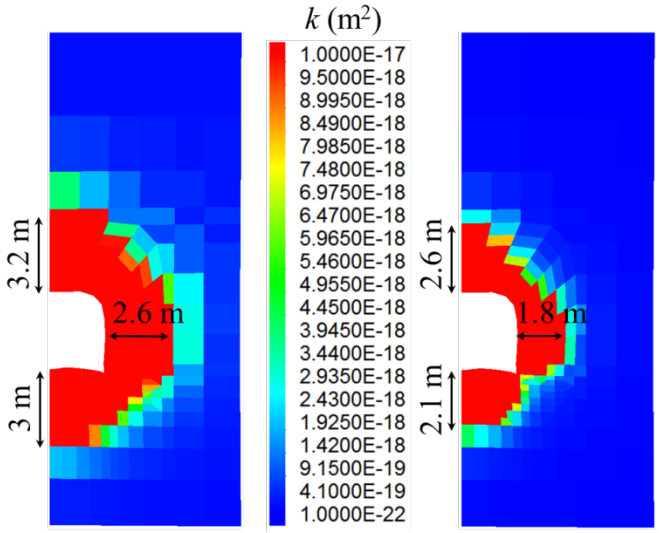

Figure 3-16. Generic Salt Repository in 2D (with solubility constraints): secondary permeability in the host rock close to the drift after 30 years.

4. DEVELOPMENT OF A PORE SCALE MODEL FOR MIGRATION OF BRINE INCLUSIONS IN SALT CRYSTALS IN THERMAL GRADIENTS

In this section, we discuss the development of a pore scale model to simulation of the migration of brine inclusions in salt crystals in thermal gradients. Previous models for brine migration in thermal gradients have used single- or dual-continuum approaches (Olivella et al. 1994; Kuhlman and Malama 2013, Rutqvist et al, 2014). In these approaches, the porous medium is conceptualized as a continuum, i.e. each point in space is assigned bulk properties that characterize this continuum (e.g. porosity, permeability) using the representative elemental volume (REV) concept. In contrast, in the pore scale approach, each point in space is assigned either to the solid or fluid phases; thus, there is no need to consider bulk properties for the porous medium. Rather, the size and shape of brine inclusions, and thus the solid-fluid interfaces are considered explicitly. Pore scale modeling constrained by pore scale observations (e.g. Caporuscio et al. 2013) can provide a useful tool to inform constitutive relationships applicable at the continuum scale.

We begin by discussing the need for understanding brine migration under thermal gradients. In the next section, we present the necessity for a pore scale approach for understanding brine migration in salt formations. We then develop the mass and momentum conservation equations for brine inclusion migration in salt crystals. This is followed by development of mathematical expressions for reactive transport equations fluxes, under thermal gradients and a discussion of the implementation of these equations in the Chombo-Crunch pore scale code.

4.1 Background

In future nuclear waste repositories groundwater is considered to be the main agent for corrosion of waste packages, solubilization of the waste forms, and transport of the wastes to the accessible environment. Natural salt deposits have low permeability and are thus excellent candidates for hosting heat-emanating wastes (e.g., used nuclear fuels). However, they will still contain a certain amount of water, either deposited with the salt or emplaced during some secondary

process. This water may be present in intercrystalline pore space, intracrystalline inclusions, and hydrated or hydrous minerals. The significance of the presence of brine in salt rock is that, under a temperature, pressure, and/or chemical potential gradient, such water has been shown to migrate. The brine volumes can move either up or down a gradient, depending upon its occurrence. . Therefore, despite the basic impermeability of salt rock, brine may still reach the waste packages and compromise their performance under repository-induced conditions (Kelly 1985).

In the past, brine-migration research for nuclear waste disposal has focused primarily on brine inclusion migration caused by thermal gradients (e.g., Anthony and Cline 1971; Jenks and Claiborne 1981; Roedder and Chou 1982; Yagnik 1983; Olander 1984). These previous investigations show that when a temperature gradient is applied to an all-liquid inclusion, migration is driven by solubility differences. Because the solubility of salt increases with temperature, salt will dissolve at the interface closest to the heat source (the "hot" face), diffuse through the brine as a result of solution composition and temperature gradients, and precipitate at the interface furthest from the heat source (the “cold” face). This is brought about because the thermal conductivity of the salt is higher than that of the brine, which produces a higher temperature gradient within the liquid than the applied gradient to the solid (Yagnik 1983). Thus, the inclusions tend to migrate toward the heat source. A number of mathematical expressions have been developed (Anthony and Cline 1971; Jenks and Claiborne 1981; Yagnik 1983; Olander 1984) for estimating the brine-inclusion-migration velocities up a thermal gradient.

4.2 Recent Pore Scale Observations

Caporuscio et al. (2013) examined brine inclusion migration in single salt crystals and salt aggregates as a function of thermal gradients. They found that at temperatures larger than 160 °C all inclusions became two-phase inclusions. In such two-phase inclusions, they observed brine to migrate up the thermal gradient, while the gas migrated down the thermal gradient. Furthermore, they found that brine inclusion migration velocity depended on the magnitude of the thermal gradient within the inclusion, the temperature of the hot face of the inclusion, the size of the inclusion, and the chemical composition of the brine. Even though these experimental observations are strictly valid for inclusion migration within a single salt crystal, they are nonetheless important results for building a reliable conceptual model of brine migration at the continuum scale. Experiments reported by Caporuscio et al. (2013) have served as conceptual basis for the development of our pore scale model. Ongoing work is focusing on calibration of reactive parameters to match observed migration rates in these experiments.

4.3 Conceptual Model

The model developed here conceptualizes the simulation domain as being composed of salt and brine (Figure 4-1. (a)). The fluid–solid boundary ($\Gamma(\boldsymbol{x})$) is represented by a level set of a function $\phi(\boldsymbol{x}, t)$ such that:

$$\Gamma = \{x | \phi(\boldsymbol{x}, t) = c\} \tag{4.1}$$

where c is a constant, and the level-set function ϕ is greater than c for brine, and less than c for the solid phase (salt). A thermal gradient is prescribed along the X axis. As a result of the temperature gradient, a difference is established in the solubility of salt between the hot and cold

faces of the inclusion. This drives dissolution at the hot face and precipitation at the cold face. As a result of the temperature gradient, a difference is established in the solubility of salt between the hot and cold faces of the inclusion. This drives dissolution at the hot face and precipitation at the cold face. As a result, the shape of the inclusion changes and concentration gradients are established within the inclusion. These gradients (reflected in the saturation index contours of Figure 4-1.(b)) drive transport of product species from the dissolving face to the cold face, where they are reactants in the precipitation reaction. These gradients continue to drive dissolution at the hot face and precipitation at the cold face, hence, resulting in the net migration of the inclusion.

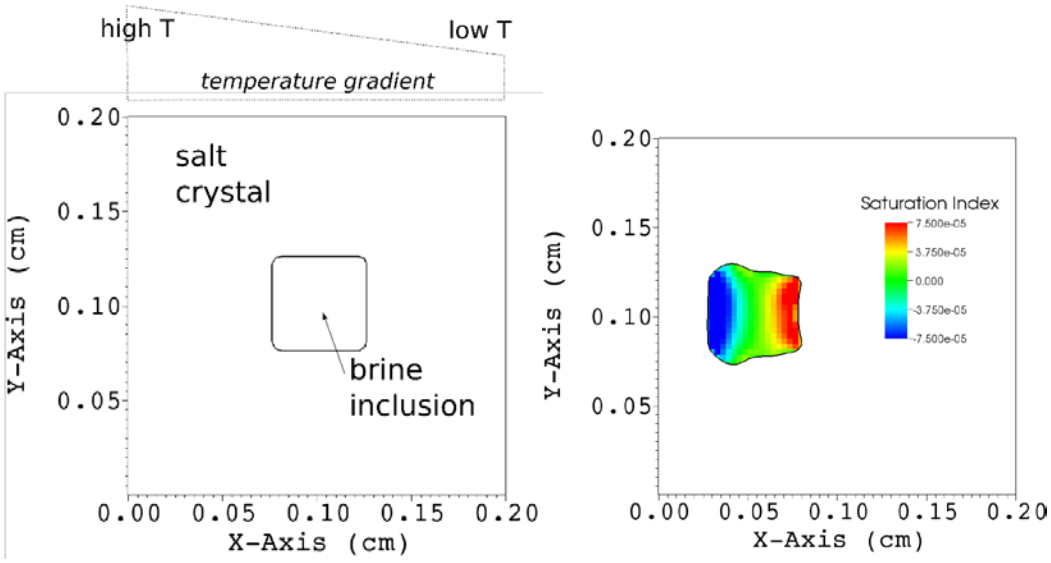

(a) **(b)**

Figure 4-1. (a) Conceptual diagram that is the basis of the pore scale model. Spatial dimensions shown are those used in preliminary simulations, with the size of the brine inclusion (5 mm) derived from the experiments of Caporuscio et al. (2013) (c.f. Fig. 37 in Caporuscio et al. (2013)). (b) Preliminary simulation results showing the shape and position of a brine inclusion migrating in a single crystal of halite, with the thermal gradient extracted from Fig 16 in Caporuscio et al. (2013). Small gradients in the degree of saturation of the brine with respect to halite drive the migration of the inclusion up the temperature gradient. Negative saturation indices indicate undersaturated conditions and drive dissolution, while positive values drive precipitation.

4.4 Governing Equations

The incompressible Navier–Stokes equations are used to accurately describe single-phase flow of water in the inclusion via the conservation of momentum and mass, respectively:

$$\rho\left(\frac{\partial \mathbf{u}}{\partial \mathrm{t}} + (\mathbf{u}\cdot\nabla)\mathbf{u}\right) = -\nabla p + \mu\nabla^2\mathbf{u} \tag{4.2}$$

$$\nabla\cdot\mathbf{u} = 0 \tag{4.3}$$

where the left-hand side of Eq. (4.2) describes the inertial forces, and the right-hand side includes the pressure gradient (∇p) and the viscous forces, with **u** being the fluid velocity, ρ the fluid density, and μ the dynamic viscosity. Inertial forces have their origin in the convective acceleration of the fluid as it flows through the tortuous pore space. Viscous forces originate in the friction between water molecules and are responsible for the dissipation of energy.

Transport and reaction of dissolved species in the brine are described by the following conservation equation:

$$\frac{\partial}{\partial t}\left(\rho M_{\mathrm{H_2O}} c_i\right) + \nabla \cdot \left(\mathbf{u}\rho M_{\mathrm{H_2O}} c_i - D_i \nabla\left(\rho M_{\mathrm{H_2O}} c_i\right)\right) = R_i \tag{4.4}$$

where c_i is the molal concentration of species i in solution (mol $kg^{-1}H_2O$), M_{H_2O} is the mass fraction of water (kg H_2O kg^{-1}), D_i is the diffusion coefficient (m^2 s^{-1}) and R_i is the reaction term (mol m^3 s^{-1}). In Equation (), transport takes place by advection (the translation in space of dissolved or suspended material at the rate of movement of a bulk fluid phase) and diffusion (mixing of solutes in the multicomponent mixture driven by concentration gradients).

Surface reactions are expressed as a boundary condition at the solid–fluid boundaries (**Γ**):

$$-D_i\left(\nabla \rho M_{\mathrm{H_2O}} c_i\right) = \xi_{im} r_m \tag{4.5}$$

where r_m is the surface reaction rate (expressed in units of mass per unit time per unit surface) and ξ_{im} is the stoichiometric coefficient of the i-th component in each surface reaction m.

For the dissolution–precipitation of salt mineral, the transition state theory law is employed:

$$r_m = k_m \exp\left[-\frac{E_a}{RT}\right] \prod a_i^n \left[1 - \exp\left(m_2 \left(\frac{\Delta G}{RT}\right)^{m_3}\right)\right] \tag{4.6}$$

where k_m is the intrinsic rate constant (mol m^{-2} reactive surface s^{-1}), E_a is the activation energy (kcal mol^{-1}), $\prod a_i^n$ is a product representing the inhibition or catalysis of the reaction by various ions in solution raised to the power n, with a_i being the activity of species I, ΔG is the Gibbs free energy (kcal) with m_1, m_2, and m_3 being three parameters that affect the affinity dependence, R is the ideal gas constant (kcal K^{-1} mol^{-1}), and T is the temperature (K). The temperature dependence of the near-equilibrium term (last term in Eq. (4.6)

Dissolution and precipitation of salt minerals such as halite change the geometry of the brine inclusion. Mathematically, dissolution and/or precipitation can be formulated as a moving boundary, or Stefan problem. Assuming uniform dissolution–precipitation of a single-mineral solid phase (m) (e.g. halite), the velocity of the moving solid–fluid interface (u_n^Γ) can be described by:

$$u_n^\Gamma = \mathbf{u}^\Gamma \cdot \boldsymbol{n} = V_m\, r_m \tag{4.7}$$

where V_m is the molar volume of the mineral. Equation (4.7) is solved along with Eqs. (4.2, 4.3, 4.4, 4.5 and 4.6).

4.5 Numerical Formulation

The governing equations were implemented in the Chombo-Crunch code, which uses an embedded boundary-algebraic multigrid formulation based on a finite volume discretization (Molins et al, 2012, Molins et al., 2014, Trebotich et al., 2014). The pore scale model developed here thus employs the so-called direct numerical simulation approach with the use of conventional discretization methods to solve the flow, transport, and geochemical equations. An operator splitting approach is used to couple flow, transport, reactions and brine-salt interface evolution. Solid-fluid interfaces are represented as embedded boundaries within each of the grid cells. The resulting cut cells are discretized by a finite volume method that accounted for the partial volumes occupied by both fluid and solid, and for the interfacial area between fluid and solid. Conservation equations are solved using a predictor-corrector projection method. A higher-order upwind method with a van Leer flux limiter is applied to advection terms in a semi-implicit Crank-Nicolson approach to minimize numerical dispersion. The movement of the interface is calculated using the approach outlines in Miller and Trebotich (2012). In this approach, the space-time discretization of divergence theorem is used to capture the time evolution of the brine-salt interface.

5. CONCLUSIONS

The FY2015 we have conducted further verification, validation, application, of the TOUGH-FLAC model, initiated pore-scale (or micro-) modeling of salt inclusion migration, as well as several publications of our work in international peer-reviewed journals. The model development of TOUGH-FLAC for salt has reached sufficient maturity for state-of-the-art applications on coupled THM processes in salt, and we have therefore been able to publish two new journal papers (Blanco Martin et al. 2015a; 2015b), which showcase the work and contribute to the state-of-the-sciences in the international salt research community.

Another major accomplishment in FY2015 is the first full 3D (86,000 elements) TOUGH-FLAC modeling of salt repository (heater experiment); it is the modeling of the Thermal Simulation for Drift Emplacement (TSDE) test that was a major multi-year heater experiment conducted at Asse Mine in Germany in the 1990s. This is the first time this experiment has been modeled with complete THM models (previous analyses of TSDE have been limited thermal-mechanical processes, ignoring multiphase flow hydraulic processes. The modeling of the experiment was conducted in collaboration with TUC and this also provided further code-to-code verification of TOUGH-FLAC. The modeling of the TSDE also provides the opportunity to calibrate of stationary creep parameters at very low deviatoric stress and extremely slow loading that are not available from current laboratory tests. Good agreement was achieved between modeled and experimental data, involving drift closure and compaction of the EBS (crushed salt), thus providing validation of both host rock and crushed salt constitutive models and their implementation into the TOUGH-FLAC simulator.

In FY2015 we have also extended TOUGH-FLAC for considering salt precipitation and dissolution, including an improved TOUGH2 equation-of-state module. This model capability was demonstrated for the generic repository model, showing the evolution of porosity in the EBS as a function of both salt precipitation and dissolution and mechanical compaction, affected by the thermal gradient and two-phase flow heat pipe effects. This model capability is currently being validated against laboratory data involving experiments with thermal gradient and monitoring of moisture content and porosity evolution.

Finally, in FY2015, LBNL has continued the work on the development of a constitutive model for migration of brine inclusions considering both pressure and thermal gradients. As part of this development LBNL have in FY2015 initiated pore-scale modeling of brine inclusion migration in salt crystals under thermal gradients. In this approach, the brine inclusions are modeled explicitly, including reactive mass transport under thermal gradients with dissolution and precipitation at hot and cold faces of the inclusions. The governing equations were implemented in the Chombo-Crunch code, which uses an embedded boundary-algebraic multigrid formulation based on a finite volume discretization. The experiments reported by Caporuscio et al. (2013) have served as conceptual basis for the development of our pore scale model. Ongoing work is focusing on calibration of reactive parameters to match observed migration rates in these experiments.

Thus, FY2015 accomplishments are summarized as follows:

- Two peer-reviewed journal papers published (after thorough journal reviews)
- Conducted the first full 3D (86,000 elements) TOUGH-FLAC modeling of salt THM processes associated with the modeling of the TSDE experiment.
- Further ode-to-code verification of TOUHG-FLAC and FLAC-TOUGH codes in collaboration with the Clausthal group achieving good agreement and confidence in respective simulators.
- Updated simulations on long-term THM evolution for a salt-based repository with using improved models of host rock and backfill with results summarized in published journal papers.
- Extended TOUGH-FLAC salt modeling to considering salt precipitation and dissolution (THMC)
- Validate the salt precipitation and dissolution modeling against experiments on crushed salt under thermal gradient.
- Initiated pore-scale modeling of brine inclusion migration under thermal gradient based on Caporuscio's brine inclusion experiments.

In FY2016, LBNL will continue to test and apply computational models and tools to simulate coupled THM processes and brine migration in salt. LBNL's modeling work will be based on the extended TOUGH-FLAC model, which incorporated new constitutive models for the damage evolution of salt and also new capabilities for simulating large deformations. LBNL will also explore the possibility of extending the TOUGH-FLAC model to THMC.

Specific objectives of the FY2016 research may include:

- Model a heater test conducted in rooms A&B at WIPP in the 1980s, to evaluate the capabilities of TOUGH-EWASG (and TOUGH-FLAC) to model brine migration in natural salt in field conditions
- Revisit the Generic Salt Repository in 2D and perform THM modeling using crushed salt and natural salt parameters derived from the modeling of the TSDE test, and also including halite dissolution/precipitation effects

- Compare simulation results using sequential and fully coupled approaches (TOUGH-FLAC and CODE_BRIGHT), to investigate the differences in terms of physical processes modeled, as well as in terms of numerical efficiency
- Continue fruitful collaboration with TU Clausthal and Prof. Lux's team, and perform further benchmark exercises regarding the disposal of heat-generating nuclear waste in saliferous formations (natural salt host rock and crushed salt backfill).
- Continue to develop the pore-scale analysis and explore the effect of physical and mineralogical heterogeneity in salt grain on the rates of migration.
- Implementation of (dual continuum) constitutive model in TOUGH-FLAC for brine migration under thermal and pressure gradients using information gained from the pore-scale modeling and experiments.

6. ACKNOWLEDGMENTS

Funding for this work was provided by the Used Fuel Disposition Campaign, Office of Nuclear Energy, of the U.S. Department of Energy under Contract Number DE-AC02-05CH11231 with Lawrence Berkeley National Laboratory.

7. REFERENCES

Andersen, G., A. Probst, L. Murray and S. Butler. 1992. An accurate PVT model for geothermal fluids as represented by H_2O-NaCl-CO_2 mixtures. In *Proceedings 17th Workshop on Geothermal Reservoir Engineering, Stanford, CA*: 239-248.

Anthony, T.R. and H.E. Cline, 1971. The thermal migration of liquid droplets through solids, Journal of Applied Physics, 42:3380–3387.

Battistelli, A., C. Calore and K. Pruess. 1993. A fluid property module for the TOUGH2 simulator for saline brines with non-condensable gas. In *Proceedings 18th Workshop on Geothermal Reservoir Engineering, Stanford,* 249-259.

Battistelli, A., C. Calore and K. Pruess. 1997. The simulator TOUGH2/EWASG for modelling geothermal reservoirs with brines and a non-condensible gas. *Geothermics* 26(4): 437-464.

Battistelli, A. 2012. Improving the treatment of saline brines in EWASG for the simulation of hydrothermal systems. In *Proceedings TOUGH Symposium 2012, Berkeley, 17-19 September 2012*.

Bechthold W, Rothfuchs T, Poley A, Ghoreychi M, Heusermann S, Gens A et al. Backfilling and Sealing of Underground Repositories for Radioactive Waste in Salt (BAMBUS Proj). Eur Atomic Energy Community, 1999. Rep EUR19124 EN.

Bechthold W, Smailos E, Heusermann S, Bollingerfehr W, Bazargan Sabet B, Rothfuchs T. Backfilling and Sealing of Underground Repositories for Radioactive Waste in Salt (BAMBUS II Proj). Eur Atomic Energy Community, 2004. Rep EUR20621 EN.

Blanco-Martín L, Rutqvist J, Birkholzer JT. Long-term modelling of the thermal-hydraulic-mechanical response of a generic salt repository for heat generating nuclear waste. Eng Geol 2015a;193:198-211. doi:10.1016/j.enggeo.2015.04.014.

Blanco-Martín L., R. Wolters, J. Rutqvist, K.-H. Lux and J.T. Birkholzer. 2015b. Comparison of two simulators to investigate thermal-hydraulic-mechanical processes related to nuclear waste isolation in saliferous formations. *Compt. Geotech.* 66:219-229.

Broome ST, Bauer SJ, Hansen FD. Reconsolidation of Crushed Salt to 250 °C Under Hydrostatic and Shear Stress Conditions. In: Proc 48th US Rock Mech/Geomech Symp, Minneapolis, 2014. Paper 14-7088.

Callahan, G.D. and K.L. DeVries. 1991. *Analyses of Backfilled Transuranic Waste Disposal Rooms*. Report SAND-91-7052: RE/SPEC Inc. (Prepared for Sandia National Laboratories), Rapid City, SD (USA).

Camphouse, R.C., M. Gross, C.G. Herrick, D.C. Kicker and B. Thompson. 2012. *Recommendations and Justifications of Parameter Values for the Run-of-Mine Salt Panel Closure System Design Modeled in the PCS-2012 PA*. Final memo: Sandia National Laboratories, Albuquerque, NM (USA).

Caporuscio, F.A., H. Boukhalfa, M.C. Cheshire, A.B. Jordan, and Ding, M., 2013. Brine migration experimental studies for salt repositories, LA-UR-13-27240, Los Alamos National Laboratory, Los Alamos, NM.

Carter, J., A. Luptak and J. Gastelum. 2011. *Fuel Cycle Potential Waste Inventory for Disposition*. Report FCR&D-USED-2010-000031 Rev 5: Prepared for US DOE Used Nuclear Fuel (USA).

Cinar, Y., Pusch, G., Reitenbach, V., 2006. Petrophysical and Capillary Properties of Compacted Salt. Transp. Porous Med. 64, 199–228. doi: 10.1007/s11242-005-2848-1.

Coussy, O. 2004. *Poromechanics*. 1st ed. Chichester: John Wiley and Sons.

DBE. Numerische Untersuchungen zum Konvergenzverhalten eines Einzelhohlraumes. DBE Technology GmbH, 2001. Rep 22341011.

Doherty J. PEST: Model-Independent Parameter Estimation. Brisbane: Watermark Numerical Computing; 2008.

Driesner, T. and C.H. Heinrich. 2007. The system H_2O-NaCl. Part I: Correlation formulae for phase relations in temperature-pressure-composition space from 0 to 1000 °C, 0 to 5000 bar, and 0 to 1 X_{NaCl}. *Geoc. Cosm. Acta* 71: 4880-4901.

Driesner, T. 2007. The system H_2O-NaCl. Part II: Correlations for molar volume, enthalpy, and isobaric heat capacity from 0 to 1000 °C, 1 to 5000 bar, and 0 to 1 X_{NaCl}. *Geoc. Cosm. Acta* 71: 4902-4919.

Finsterle S. iTOUGH2 User's Guide. Lawrence Berkeley Natl Lab, Berkeley, 2007. Rep LBNL-40040.

Finsterle S, Zhang Y. Solving iTOUGH2 simulation and optimization problems using the PEST protocol. Environ Modelling Softw 2011;26(7):959-68. doi:10.1016/j.envsoft.2011.02.008.

Hou Z. Mechanical and hydraulic behaviour of rock salt in the excavation disturbed zone around underground facilities. Int J Rock Mech Min Sci 2003;40:725-38. doi:10.1016/S1365-1609(03)00064-9.

Itasca. FLAC3D (Fast Lagrangian Analysis of Continua in 3 Dimensions), Version 5.0. Minneapolis: Itasca Consulting Group; 2012.

Jenks, G.H., and H.C. Claiborne, 1981. Brine migration in salt and its implications in the geologic disposal of nuclear waste, ORNL-5818, Oak Ridge National Laboratory, Oak Ridge, TN.

Jové-Colón, C., J.A. Greathouse, S. Teich-McGoldrick, R.T. Cygan, T. Hadgu, J.E. Bean, M.J. Martínez, P.L. Hopkins, J.G. Argüello and F.D. Hansen. 2012. *Evaluation of Generic EBS*

Design Concepts and Process Models: Implications to EBS Design Optimization. Report FCRD-USED-2012-000140: Sandia National Laboratories, Albuquerque, NM (USA).

Jordan, A.B.; Boukhalfa, H.; Caporuscio, F.A.; Robinson, B.A.; Stauffer, P.H. Hydrous mineral dehydration around heat-generating nuclear waste in bedded salt formations, *Environ. Sci. & Technol.* 2015, 49, 6783-6790.

Kachanov LM. Introduction to Continuum Damage Mechanics. 1st ed. Dordrecht: Martinus Nijhoff Publishers; 1986.

Kröhn KP, Zhang CL, Wolf J, Stührenberg D, Jobmann M, von Borstel L, Lerch C. The compaction behaviour of salt backfill at low porosities. In: Proc 7th Int Conf Mech Behav Salt (SaltMech7), Paris, 2012. p. 155-62.

Kuhlman, K.L., and B. Malama, 2013. Brine flow in heated geologic salt, SAND2013-1944, Sandia National Laboratory, Albuquerque, NM.

Kuhlman, K.L. 2014. S*ummary Results for Brine Migration Modeling Performed by LANL, LBNL and SNL for the UFD Program*. Report FCRD-UFD-2014-000071: Sandia National Laboratories (Prepared for US DOE UFD), Albuquerque, NM (USA).

Lerche S. Kriech- und Schädigungsprozesse im Salinargebirge bei mono- und multizyklischer Belastung. Ph.D. Dissertation, TU Clausthal; 2012.

Leverett, M. C., 1941. Capillary behaviour in porous solids. Petroleum Transactions, AIME(192), 152-169.

Lux K-H, Rutenberg M, Seeska R, Düsterloh U. Kopplung der Softwarecodes FLAC3D und TOUGH2 in Verbindung mit in situ-, laborativen und numerischen Untersuchungen zum thermisch-hydraulisch-mechanisch gekoppelten Verhalten von Tongestein unter Endlagerbedingungen. TU Clausthal, 2015. Final Rep BMWi-Proj 02E11041.

Miller G.H. and Trebotich D., "An Embedded Boundary Method for the Navier-Stokes Equations on a Time-Dependent Domain", Communications in Applied Mathematics and Computational Science, 7(1):1-31, 2012,

Millington RJ, Quirk JP. Permeability of Porous Solids. Transactions Faraday Soc 1961;57:1200-07. doi: 10.1039/TF9615701200.

Molins S, Trebotich D, Steefel CI, Shen C (2012) An investigation of the effect of pore scale flow on average geochemical reaction rates using direct numerical simulation. Water Resour Res 48: WR03527

Molins S, Trebotich D, Yang L, Ajo-Franklin JB, Ligocki TJ, Shen C, Steefel CI (2014) Pore-scale controls on calcite dissolution rates from flow-through laboratory and numerical experiments. Environ Sci Technol 48:7453–7460

Nowak EJ. 1986. Preliminary results of birne migration studies in the Waste Isolation Pilot Plant (WIPP). Report SAND-86-0720: Sandia National Laboratories, Albuquerque, NM (USA).

Nowak EJ and McTigue DF. 1987. Interim results of brine transport studies in the Waste Isolation Pilot Plant (WIPP). Report SAND -87-0880: Sandia National Laboratories, Albuquerque, NM (USA).

Olander, D.R., 1984. A study of thermal-gradient induced migration inclusions in salt: Final report, BMI/ONWI-538, Regents of the University of California, Oakland, CA.

Olivella, S., J. Carrera,, A Gens, E.E. Alonso, 1994. Nonisothermal multiphase flow of brine and gas through saline media, Transport in Porous Media, 15:271–293.

Olivella S, Carrera J, Gens A, Alonso EE. 1996. Porosity Variations in Saline Media Caused by Temperature Gradients Coupled to Multiphase Flow and Dissolution/Precipitation. Transp Porous Med 25:1-25.

Olivella S, Castagna S, Alonso EE and Lloret A. 2011. Porosity variations in saline media induced by temperature gradients: experimental evidences and modelling. Transp Porous Med 90:763-777.

Palliser, C. and R. McKibbin. 1998. A Model for Deep Geothermal Brines, I: *T-P-X* State-Space Description. *Transp. Porous Med.* 33: 65-80.

Phillips, S.L., A. Igbene, J.A. Fair, H. Ozbek and M. Tavana. 1981. *A technical databook for geothermal energy utilization*. Report LBL-12810: Lawrence Berkeley Laboratory, Berkeley, CA (USA).

Popp T, Kern H, Schulze O. Evolution of dilatancy and permeability in rock salt during hydrostatic compaction and triaxial deformation. J Geophys Res 2001;106(B3):4061-78. doi: 10.1029/2000JB900381.

Pruess, K., C. Oldenburg and G. Moridis. 2011. *TOUGH2 User's Guide, Version 2.0.* Report LBNL-43134: Lawrence Berkeley National Laboratory, Berkeley, CA (USA).

Pudewills A, Droste J. Numerical modeling of the thermomechanical behavior of a large-scale underground experiment. Comput Struct 2003; 81(8-11):911-18. doi:10.1016/S0045-7949(02)00427-3.

Rege, S.D. and Fogler H.S. 1989. Competition among flow, dissolution and precipitation in porous media. AIChE J. 35(7):1177-1185.

Roedder, E., and L.M. Chou, 1982. A critique of "Brine migration in salt and its implications in the geologic disposal of nuclear waste," Oak Ridge National Laboratory Report 5818, by G.H. Jenks and H.C. Claiborne, USGS Open-File Report 82-1131.

Rutqvist, J., Blanco Martín, L., Mukhopadhyay, S., Houseworth, J. Birkholzer, J. (August 2014) Modeling Coupled THMC Processes and Brine Migration in Salt at High Temperatures, LBNL-6718E, Lawrence Berkeley National Laboratory.

Rutqvist, J., Y.S. Wu, C.F. Tsang and G. Bodvarsson. 2002. A Modeling Approach for Analysis of Coupled Multiphase Fluid Flow, Heat Transfer, and Deformation in Fractured Porous Rock. *Int. J. Rock Mech. Min. Sci*. 39: 429-442.

Rutqvist J., L. Blanco Martín, J. Kim, and J.T. Birkholzer, 2013. Modeling Coupled THMC Processes and Brine Migration in Salt at High Temperatures. Report FCRD-UFD-2013-000262.

Rutqvist 2014 - Modeling and Field Test Planning Activities in Support of Disposal of Heat-Generating Waste in Salt. Report FCRD-UFD-2014-000622.

Rycroft CH. Voro++: a three-dimensional Voronoi cell library in C++. http://math.lbl.gov/voro++/ (2009).

Sjaardema, G.D. and R.D. Krieg. 1987. *A Constitutive Model for the Consolidation of WIPP Crushed Salt and Its Use in Analyses of Backfilled Shaft and Drift Configurations*. Report SAND-87-1977: Sandia National Laboratories, Albuquerque, NM (USA).

Stauffer, P.H., D.A. Harp, A.B. Jordan, Z. Lu, S. Kelkar, Q. Kang, J. Ten Cate, H. Boukhalfa, Y, Labyed, P.W. Reimus, F.A. Caporuscio, T.A. Miller and B.A. Robinson. *Coupled model for heat and water transport in a high level waste repository in salt.* Report M2FT-13LA08180113: Los Alamos National Laboratory (Prepared for US DOE UFD), Los Alamos, NM (USA).

Stauffer, P.H., A.B. Jordan, D.A. Harp, G.A. Zyvoloski, H. Boukhalfa, F.A. Caporuscio, T.A. Miller and B.A. Robinson. *Thermo-Hydrological and Chemical (THC) Modeling to Support Field Design Test.* Report M4FT-14LA0818064: Los Alamos National Laboratory (Prepared for US DOE UFD), Los Alamos, NM (USA).

Trebotich D, Adams MF, Molins S, Steefel CI, and Shen C. (2014) High-resolution simulation of pore-scale reactive transport processes associated with carbon sequestration. Comput Sci Engin 16(6):22–31

Trebotich D, Graves DT (2015) An adaptive finite volume method for the incompressible Navier-Stokes equations in complex geometries. Comm Appl Math Comput Sci, 10-1:43-82, doi: 10.2140/camcos.2015.10.43

Vargaftik NB. Tables on the Thermophysical Properties of Liquids and Gases. 2nd ed. New York: Hemisphere Publishing; 1975. doi: 10.1002/aic.690210636.

van Genuchten, M.T., 1980. A closed-form equation for predicting the hydraulic conductivity of unsaturated soils. Soil Sci. Soc. Am. J. 44(5), 892-898. doi: 10.2136/sssaj1980.03615995004400050002x.

Walker, W.R., Sabey, J.D., Hampton, D.R., 1981. Studies of Heat Transfer and Water Migration in Soils. Department Agric. Chem. Eng., Colorado State University, Fort Collins, CO, USA. Final Rep., 140 pp.

Wolters R, Lux K-H, Düsterloh U. Evaluation of Rock Salt Barriers with Respect to Tightness: Influence of Thermomechanical Damage, Fluid Infiltration and Sealing/Healing. In: Proc 7th Int Conf Mech Behav Salt (SaltMech7), Paris, 2012. p. 425-34.

Yagnik, S. K., 1983. Interfacial stability of migrating brine inclusions in alkali halide single crystals supporting a temperature gradient, Journal of Crystal Growth, 62:612-626.